

# Integrating brain and biomechanical models - a new paradigm for understanding neuro-muscular control

**Sebastian James**<sup>1,2</sup>, **Chris Papapavlou**<sup>5</sup>, **Alexander Blenkinsop**<sup>1,2</sup>,  
**Alexander Cope**<sup>3</sup>,

**Sean Anderson**<sup>2,4</sup>, **Konstantinos Moustakas**<sup>5</sup>, **Kevin Gurney**<sup>1,2,\*</sup>

<sup>1</sup> *Adaptive Behaviour Research Group, Department of Psychology, The University of Sheffield, Sheffield, UK*

<sup>2</sup> *Insigneo Institute for in-silico Medicine, The University of Sheffield, Sheffield, UK*

<sup>3</sup> *Department of Computer Science, The University of Sheffield, Sheffield, UK*

<sup>4</sup> *Department of Automatic Control Systems Engineering, The University of Sheffield, Sheffield, UK*

<sup>5</sup> *Department of Electrical and Computer Engineering, The University of Patras, Patras, Greece*

Correspondence\*:

Kevin Gurney

Department of Psychology, The University of Sheffield, Western Bank, Sheffield, S10 2TP, UK, k.gurney@sheffield.ac.uk

## 2 ABSTRACT

To date, realistic models of how the central nervous system governs behaviour have been restricted in scope to the brain, brainstem or spinal column, as if these existed as disembodied organs. Further, the model is often exercised in relation to an *in vivo* physiological experiment with input comprising an impulse, a periodic signal or constant activation, and output as a pattern of neural activity in one or more neural populations. Any link to behaviour is inferred only indirectly via these activity patterns. We argue that to discover the principles of operation of neural systems, it is necessary to express their behaviour in terms of physical movements of a realistic motor system, and to supply inputs that mimic sensory experience. To do this with confidence, we must connect our brain models to neuro-muscular models and provide relevant visual and proprioceptive feedback signals, thereby closing the loop of the simulation. This paper describes an effort to develop just such an integrated brain and biomechanical system using a number of pre-existing models. It describes a model of the saccadic oculomotor system incorporating a neuromuscular model of the eye and its six extraocular muscles. The position of the eye determines how illumination of a retinotopic input population projects information about the location of a saccade target into the system. A pre-existing saccadic burst generator model was incorporated into the system, which generated motoneuron activity patterns suitable for driving the biomechanical eye. The model was demonstrated to make accurate saccades to a target luminance under a set of environmental constraints. Challenges encountered in the development of this model showed the importance of this integrated modelling approach. Thus, we exposed shortcomings in individual model components which were only apparent when these

were supplied with the more plausible inputs available in a closed loop design. Consequently we were able to suggest missing functionality which the system would require to reproduce more realistic behaviour. The construction of such closed-loop animal models constitutes a new paradigm of *computational neurobehaviour* and promises a more thoroughgoing approach to our understanding of the brain's function as a controller for movement and behaviour.

Keywords: integrated brain biomechanics neuromuscular oculomotor saccade basal ganglia

## 1 INTRODUCTION

Note: Changes based on Reviewer 1's comments are in this colour. For Reviewer 2 we use this colour.

The field of computational neuroscience has provided many *systems models* of the brain (Arai et al., 1994; Gancarz and Grossberg, 1998; Hazy et al., 2007; Blenkinsop et al., 2017). We refer to these as *mechanistic computational models*, meaning models which consist of populations of neural elements, interconnected in a biologically plausible manner, which simulate the operation of the brain. Whilst they differ in scale and complexity, these models all seek to describe the fundamental mechanisms behind common animal behaviours such as locomotion, threat evasion, reaching or feeding. However, none of the models cited here actually reproduce these behaviours. In each case, the activity in a certain population of neurons is taken to be representative of a behavioural outcome. In some cases, it is reasonable to take the activity of an internal population within the brain model as being representative of the induced behaviour. For example, a choice made in a *go/no-go* task could be determined from activity in a population within a basal ganglia model (Nambu et al., 1990; Kühn et al., 2004). The decision to *go* is selected by a reduction of activity in this population; maintenance of activity implies *no-go*. To validate the model, the error rates which it generates could be compared with experimentally determined error rates in primate subjects. We refer to this as an *output assumption model* because the output is assumed to signify behaviour. (An *input assumption model* assumes that sensory input produces some particular form of neural activity in an input population of the model.)

However, we may be interested in reproducing accurate simulated *trajectories*, in order to find out how degradation of parts of the model affect movement. In Parkinson's Disease, degradation of the dopamine neurons originating in the substantia nigra pars compacta (SNc) causes diskinesia (Galvan and Wichmann, 2008), as well as abnormal network activity in the basal ganglia (Brown et al., 2001; McCarthy et al., 2011). Sufferers of the disease would be expected to produce abnormal decision-making and movement trajectories in a reach-to-the-correct-target task such as the one described in James et al. (2017). A model which sought to explore in detail the effects of the SNc degradation both on the decision making and on the movement dynamics would need a physically accurate virtual arm, as well as physically realistic sensory input for the brain. This is no less than a complete model of those sections of the brain and body which act to fulfil the task. Such a modelling effort, if successful, would result in a virtual robot capable of expressing behaviour in response to sensory input from its environment. This would represent a paradigm shift in the field of computational neuroscience worthy of the new name of *computational neurobehaviour*.

In an attempt to build a model combining brain, realistic biomechanics and sensory feedback, we sought to extend our previous work modelling the oculomotor system by adding a virtual, biomechanical eye model able to make physically realistic movements. The rotational state of the eye would then determine how visual features in the virtual world were projected back into the brain model. The existing model (Cope et al., 2017) is already able to capture sensory input and convert it into a neural signal, assumed to specify the target of a *saccadic eye movement*; a fast movement of the eyes which directs the fovea to

64 a region of interest in the field of view. The oculomotor system is an excellent candidate for modelling  
65 because its movements can be specified with only three degrees of freedom, making it one of the simplest  
66 neuro-muscular systems in the body. It is nevertheless behaviourally interesting, as saccadic eye movements  
67 reveal information about decision making at a subconscious level (Deubel and Schneider, 1996; Reppert  
68 et al., 2015; Marcos and Genovesio, 2016). The modelling of the oculomotor system is served by a large  
69 body of behavioural data describing saccades (Tipper et al., 2001; Walker et al., 1997; Casteau and Vitu,  
70 2012), many anatomical studies of the neural substrates involved (Meredith and Ramoa, 1998; Isa, 2002;  
71 Isa and Hall, 2009) and electrophysiological data linking these together (Hepp and Henn, 1983; Dorris et al.,  
72 1997; McPeek et al., 2003; Vokoun et al., 2011). Furthermore, in the context of building *behaving* systems,  
73 a necessary part of any model for which the behaviour requires visual attention and decision making is a  
74 realistic mechanism for gathering visual information. This is obvious from extrinsic considerations—a  
75 subject must look at a scene to make decisions or navigate within it. It also follows for *intrinsic* reasons.  
76 For example, Howard and Tipper (1997) showed that visual cues affect reach trajectories and the same  
77 group later demonstrated that reaching affects the saccadic system (Tipper et al., 2001) suggesting a close  
78 relationship between these neural systems. **Building a behaving oculomotor system will therefore assist**  
79 **future computational neurobehavioural modelling efforts that involve reaching.**

80 Many neural populations are involved in the coding of saccadic eye movements, only a very brief  
81 overview is given here; for a review, see Munoz (2002). One pathway takes information from the retina  
82 directly into the superficial layers of the superior colliculus in the brainstem (Sterling, 1971; Linden and  
83 Perry, 1983; Wu et al., 1994). Activity within the superior colliculus then excites neurons in the pons,  
84 medulla and rostral mid-brain (Sparks, 2002). and **finally the motor neurons** which innervate the extraocular  
85 muscles (Fuchs and Luschei, 1970; Sparks, 2002). This direct pathway is responsible for the low latency  
86 saccades called express saccades (Schiller et al., 1987; Edelman and Keller, 1996). Information from the  
87 retina is also processed by visual cortex which feeds through to the frontal eye fields in which activity is  
88 related to reflexive and voluntary saccades (Schall and Thompson, 1999). Activity build-up in the frontal  
89 eye fields is transferred to the intermediate layers of the superior colliculus (Stanton et al., 1988b) and is  
90 also processed by the basal ganglia, which participates in the selection of the winning saccade end point  
91 (Stanton et al., 1988a; Hikosaka et al., 2000). Although both cortical and subcortical paths produce a  
92 saccade target signal in the superior colliculus, it is also possible for animals to make relatively normal  
93 saccades even after the colliculus has been ablated (Wurtz and Goldberg, 1972; Aizawa and Wurtz, 1998),  
94 though express saccades are lost with collicular lesions (Schiller et al., 1987). This makes the superior  
95 colliculus a perplexing structure, being both critically involved in saccade target specification (Sparks and  
96 Nelson, 1987) and saccade dynamic control (Waitzman et al., 1991; Goossens and van Opstal, 2012) and  
97 yet dispensable. The ‘backup pathway’ likely incorporates the oculomotor vermis and fastigial oculomotor  
98 region of the cerebellum which are known to participate in the specification, dynamics and adaptation of  
99 saccadic eye movements (Kleine, 2003; Takagi et al., 1998).

100 There is a long history of modelling the oculomotor system. For a comprehensive review, see Girard and  
101 Berthoz (2005). Models of individual **sub-systems** have been proposed for brainstem (Robinson, 1975;  
102 Scudder, 1988; Gancarz and Grossberg, 1998), cerebellum (Quaia et al., 1999; Dean, 1995; Dean et al.,  
103 1994) and superior colliculus (Arai et al., 1994; Morén et al., 2013; Marino et al., 2012). More recently,  
104 combined models have also been developed incorporating sensory input (Cope et al., 2017) and driving **a**  
105 **second order differential equation** representing the eye (Tabareau et al., 2007; N’Guyen et al., 2014; Thurat  
106 et al., 2015). None of these models has yet fully closed the loop to produce a behaving system operating  
107 freely within its environment. We argue that developing integrated, closed-loop models of behaving systems

108 offers insights into the operation of neural systems that are not available from input- or output-assumption  
109 models.

## 2 MATERIAL & METHODS

110 The integrated brain and biomechanical model described here is a development of the model in Cope  
111 et al. (2017), referred to here as the Cope-Chambers model. This was a rate-coded neural network model  
112 incorporating retinal populations, frontal eye fields (FEF), the basal ganglia (BG), and the superior colliculus  
113 (SC). The Cope-Chambers model takes as *input* the positions of luminances (of fixed shape and intensity)  
114 on a topographic map. Whilst certain assumptions were made about the input—that a luminant input excites  
115 activity on a retinotopic layer, with computer code carrying out the transformation achieved in the brain by  
116 a neural connectivity map (Thivierge and Marcus, 2007)—it is nonetheless *not* an input-assumption model  
117 according to our definition because the activity generated in the neural input layer is modelled as a response  
118 to the luminances, rather than being crafted. In the Cope-Chambers model, the centroid of the activity in  
119 the deep layers of superior colliculus was assumed to accurately encode the location of the eye at the end  
120 of the saccade (Wurtz and Goldberg, 1972; Robinson, 1972; Van Gisbergen et al., 1987; McIlwain, 1982).  
121 This location was used to recalculate the positions of the luminances in the eye's frame of reference at each  
122 time step. Because a pattern of neural activity in the output population was assumed to have a behavioural  
123 outcome, it was thus an *output-assumption model*. The model included no brainstem populations other  
124 than superior colliculus, nor a neuromuscular model.

125 To the Cope-Chambers model, we added a brainstem model and a biomechanical eye model. The rate-  
126 coded brainstem model was taken from the literature (Gancarz and Grossberg, 1998) as the best-of-breed  
127 saccadic burst generator (Girard and Berthoz, 2005). The biomechanical eye was implemented using the  
128 biomechanical modelling framework OpenSim; the brain and brainstem were modelled using the SpineML  
129 toolchain. These will be described below, along with a review of the Cope-Chambers model, but first we  
130 will give a description of the co-ordinate systems.

### 131 2.1 Co-ordinates in the world

132 Before describing the biomechanical eye and the brain model, which consisted of retinotopically mapped  
133 neural sheets, we describe the co-ordinate system used in the world. The eye was located at the origin of a  
134 three-dimensional, right-handed Cartesian co-ordinate system, with its fovea directed in the  $-z$  direction.  
135 There was a notional spherical screen which was also centred at the origin of the co-ordinate system and  
136 had a radius of 50 (in arbitrary units). The *fixation point* was the point on the screen at which the eye  
137 was initially directed. Onto the screen were projected target luminances, each of which having a position  
138 described by two co-ordinates;  $\theta_x^t$ , a rotation of the horizon plane about the  $x$  axis, and  $\theta_y^t$ , a rotation of the  
139 meridian plane about the  $y$  axis. The position is the intersection of these rotated planes with the spherical  
140 screen (disregarding the intersection point of these three surfaces behind the eye). Note that a luminance  
141 with positive  $\theta_x^t$  was above the horizon of this world; one whose  $\theta_y^t$  was positive lay to the left of the  
142 world's meridian. For this reason, many of the figures in this paper are plotted with  $-\theta_y$  on the  $x$ -axis and  
143  $\theta_x$  on the  $y$ -axis so that targets that lay up and to the right in the world do so in the graphs, also.

144 Luminances were crosses of height and width subtending  $\pm 3^\circ$  and whose 'bars' were  $2^\circ$  thick. Lumi-  
145 nances were oriented like + symbols with their vertical bar aligned with the meridian plane and their  
146 horizontal bar aligned with the horizon.

147 The eye's frame of reference was initially aligned with the world's frame of reference. At each timestep,  
148 the eye's rotational state (described by the Euler rotations  $\theta_x$ ,  $\theta_y$ ,  $\theta_z$ ) was used to translate the three  
149 dimensional Cartesian co-ordinates of the luminances in the world frame into co-ordinates in the eye frame.  
150 The luminance co-ordinates in the eye's frame of reference were used to determine the input to the brain  
151 model.

## 152 2.2 Existing brain model

153 The brain model, excluding the brainstem, is a re-implementation of the Cope-Chambers model, of  
154 reflexive saccadic behaviour (Cope et al., 2017). Reflexive saccades are fast eye movements elicited by  
155 abrupt changes in the peripheral visual scene (reflexive saccades can occur also as a result of auditory  
156 and somatosensory stimuli, but these modalities are ignored in this model). A reflexive saccade has a  
157 starting position defined by the initial orientation of the eye and an end-point position in which the eye  
158 is directed towards a new target. Regardless of the number of targets within the visual scene, the brain  
159 must choose one location as the end-point, because the eyes can look only in one direction at a time. The  
160 functionality reproduced by the Cope-Chambers model is 'the selection of the best target end-point for  
161 a reflexive saccade'. A competition such as this between incompatible movements is often referred to  
162 as an *action selection* problem (Norman and Shallice, 1986; Maes, 1989; Redgrave et al., 1999). The  
163 Cope-Chambers model is therefore a model of action-selection in the oculomotor system for reflexive  
164 saccades. One hypothesis for the rôle played by the basal ganglia (BG) is that the system performs *action*  
165 *selection* (Mink, 1996; Redgrave et al., 1999; Hikosaka et al., 2000). The Cope-Chambers model places the  
166 BG at the centre of the oculomotor system; this follows the known anatomy of the region (Hikosaka et al.,  
167 2000) and provides a mechanism for action selection of the best saccade. The BG receives input indirectly  
168 from the superior colliculus, which has a retinotopic arrangement (Ottos et al., 1986).

169 The BG receives excitatory inputs directly from retinotopic regions of the cortex including the frontal eye  
170 fields (FEF), supplementary eye fields (SEF), lateral intraparietal cortex (LIP) and dorsolateral prefrontal  
171 cortex. The dorsolateral prefrontal cortex, which participates in voluntary saccades (Funahashi et al., 1993;  
172 Munoz and Everling, 2004), is not modelled because the model concerns reflexive rather than voluntary  
173 eye movements. Several other regions of the brain that are associated with eye movements are also omitted  
174 from the model. The early visual processing stream in cortex, from V1, through to the LIP is subsumed into  
175 a 'sustained retinal' signal which arrives at FEF. The justification here is that the model reacts to simple  
176 luminant targets and does not need to carry out the feature extraction performed by these visual areas. The  
177 supplementary eye fields are involved in the programming of saccade sequences (Tehovnik et al., 2000)  
178 and memory guided saccades (Chen and Wise, 1995; Schlag, 2002). Lesions of SEF do not affect visually  
179 guided saccades (Gaymard et al., 1998) and so the SEF is also omitted from the model.

180 Fig. 6(a) shows the macroscopic architecture of the Cope-Chambers model. The figure shows the  
181 relationships between the retinal input populations, the FEF, the populations comprising the BG sub-system  
182 (the red border indicates that the box represents a number of populations as a sub-system), the thalamus and  
183 the superior colliculus. Excitatory connections are indicated with arrow heads; inhibitory connections with  
184 circles in place of the arrow heads. The blue and green connection lines indicate two thalamo-basal ganglia  
185 loops, one cortical loop through FEF (green), the other a sub-cortical loop through SC. It is important to  
186 note that although they are given different colours in the diagram, these loops are in no way independent,  
187 with loop activity combining both in thalamus and in the basal ganglia and a direct excitatory, feed-forward  
188 connection from FEF to SC.

189 The basal ganglia sub-system is the most complex component of the Cope-Chambers model. The BG  
190 model is based on previous work (Gurney et al., 2001b,a) and is referred to as the GPR model. The GPR model  
191 incorporates the following main components of the primate BG (Mink, 1996; Wickens, 1997): (i)  
192 The striatum (the main input station to the BG) which is divided into two iterdigitated populations of  
193 projection neurons expressing primarily D1 or D2-type dopaminergic receptors (named Str\_D1 and Str\_D2);  
194 (ii) The subthalamic nucleus (STN); (iii) the external segment of the globus pallidus (GPe); (iv) the output  
195 nucleus relevant for saccadic control—the substantia nigra pars reticulata (SNr) (Hikosaka et al., 2000).

196 The connectivity of the GPR model [Fig. 6(b)] is constrained by the known anatomy and physiology of  
197 the BG (Bolam et al., 2000). Physiologically, the only source of glutamate within the BG is the STN, whose  
198 projections are therefore excitatory; all other nuclei have GABAergic projection neurons and are therefore  
199 inhibitory. The cortex sends glutamatergic projections to both the Str\_D1 striatal population, which projects  
200 preferentially to the SNr, and to Str\_D2, which projects primarily to GPe (Gerfen et al., 1990). The cortex  
201 also projects to the STN, which sends diffuse projections to the SNr and GPe (Parent and Hazrati, 1993).  
202 The GPe projects to the SNr and also projects back to the STN, completing a GPe-STN loop.

203 The GPR model is arranged into ‘action channels’; Fig. 6(b) shows an example network containing three  
204 channels. It is between these channels that competition occurs, with the winning channel succeeding in  
205 reducing activity in the output nucleus, SNr, and thereby disinhibiting its target. The complete connectivity  
206 pattern for this small network is shown in Fig. 6(b); the left channel in cortex innervates the left channels  
207 of Str\_D1, STN and Str\_D2. Connections are one-to-one, so it follows that the middle channel of cortex  
208 innervates the middle channels of STN and the striatal populations and the right channel of cortex innervates  
209 right channels in striatum and STN. Striatal population channels also inhibit SNr and GPe on a one-to-one  
210 basis and GPe feeds inhibition to SNr and STN in a one-to-one manner. The outputs from STN however  
211 are not one-to-one. The output from all channels of STN is summed together and then the sum is fed into  
212 each channel of SNr and GPe. This models the diffuse excitation from STN which has been observed in  
213 the BG (Parent and Hazrati, 1993).

214 Within the BG, there are several mechanisms supporting competitive processing for selecting channels  
215 whose inhibitory output should be reduced. The selection mechanism of the GPR model is the ‘off-centre,  
216 on-surround’ scheme proposed by Mink and Thach (1993). The ‘on-surround’ is provided by diffuse,  
217 excitatory projections from the STN to the SNr. Focussed inhibition from the Str\_D1 neurons in striatum  
218 contributes the ‘off-centre’ part of the mechanism. This arrangement leads to selection behaviour via a  
219 release of target inhibition, since channels that have strong salience (input) have weak output at the level of  
220 SNr, and channels with weak salience have enhanced output.

221 The GPe is not included in the centre-surround circuit described above, but still plays a key rôle in  
222 selection. Operating alone, the Str\_D1/STN/SNr circuit can suffer from the following problem: if the input  
223 for all channels is relatively high, then the diffuse projection from STN, which effectively supplies a sum  
224 of *all* of the STN inputs to each channel in SNr, will provide so much excitation that Str\_D1 may become  
225 unable to inhibit one of the channels in SNr and selection may become impossible. Gurney et al. (2001b,a)  
226 showed that the inhibitory feedback from GPe to STN acts as an ‘automatic gain control’ to help prevent  
227 this from occurring.

228 At the neuronal level, the STN, GPe and SNr have tonic output levels (Chevalier and Deniau, 1990;  
229 DeLong et al., 1985; Kita and Kitai, 1991). This is modelled using piecewise linear output functions  
230 with zero offsets,  $c$  (see Eq. 4) but with noise added to the input. In striatum, Str\_D1 and Str\_D2 have  
231 positive offset  $c$ , mimicking the so-called ‘down-state’ of medium spiny neurons which have a resting

232 potential far below spiking threshold and require co-ordinated input to generate action potentials (Wilson  
233 and Kawaguchi, 1996). In addition, the Str\_D1 and Str\_D2 neurons are influenced by dopamine in different  
234 ways; facilitating cortico-striatal transmission at medium spiny neurons with D1 receptors (Hernndez-Lpez  
235 et al., 1997; Gonon, 1997) and reducing transmission at those with D2 receptors (Delgado et al., 1999).  
236 These effects are modelled using a dopamine parameter which modulates the input activation as described  
237 below in Eqs 8 & 9; Str\_D1 activation is enhanced; Str\_D2 activation is suppressed.

238 The GPR model in Fig. ??(b) has only three channels, with the focussed inhibition from striatum to SNr  
239 and GPe defined by a simple one-to-one scheme. The action channels represent discrete, incompatible  
240 motor action choices. In the oculomotor model, an action channel represents the end-point of saccade,  
241 and the competition carried out in the basal ganglia is between potential saccade end-points. However,  
242 eye movements have a *continuous* end-point space; the eye can rotate to any orientation within its  
243 biomechanically permissible range. Some end-points within this range are mutually exclusive—it's not  
244 possible to look to the left and to the right simultaneously—but *nearby* end-points are not necessarily  
245 incompatible. A small enough error in the end-point of a saccade will not prevent the eye from foveating on  
246 a target as the foveal region of high visual acuity is not infinitesimally small. To cope with this requirement,  
247 the populations within the oculomotor basal ganglia are conceived of as two-dimensional topographic  
248 grids of leaky integrator neural elements. Activity in each element corresponds to a spatial location in the  
249 visual field. Neighbouring elements correspond to locations which are close to each other in the visual field.  
250 Focussed one-to-one projections in the GPR model are replaced by projective fields with many weighted  
251 connections. Specifically, each unit in Str\_D1 projected to a counterpart SNr<sub>j</sub> in SNr with some weight  
252  $w_{max}$ , but also connected to neighbouring nodes in SNr with a weight given by  $w_{max} \cdot G(d)$ , where  $G(d)$  is  
253 a circularly symmetric, 2D-Gaussian which is a function of distance  $d$  from SNr<sub>j</sub> [Fig. 6(c)]. A similar  
254 scheme applied for the connectivity from Str\_D2 to GPe and for a number of the other connections in the  
255 Cope-Chambers model; in the SpineML implementation of the model, this connectivity scheme is named  
256 ‘GaussianKernel’. Fig. 7 shows a schematic of the SpineML implementation of the model, based on a  
257 diagram output directly from SpineCreator. Populations for Str\_D1, Str\_D2, STN, SNr and GPe are shown  
258 within the ‘Basal Ganglia’ box. Input comes into the model via the ‘World’ population and the output  
259 population is SC\_deep. Compare this diagram with Figs. ??(a) & (b). Fig. 7 expands the ‘SC’, ‘BG’ and  
260 ‘slow retinal’ boxes from Fig. ??(a).

261 The frontal eye fields (FEF) are a key cortical area for the generation of saccadic eye movements (Hikosaka  
262 et al., 2000; Tehovnik et al., 2000; Robinson and Fuchs, 1969; Bruce and Goldberg, 1985). Saccadic targets  
263 are mapped retinotopically over its surface (Robinson and Fuchs, 1969; Bruce and Goldberg, 1985; Sabes  
264 et al., 2002), and increased neural activity at a location in the map precedes a saccade to that location.  
265 Importantly, the FEF is also associated with visual decision making (Thompson and Bichot, 2005; Schall  
266 et al., 1995; Monosov et al., 2008; Cohen et al., 2009). Thus, in a saccade choice, increased FEF activity is  
267 predictive of the eye movement whether correct or incorrect (Thompson et al., 2005), rather than of the  
268 correct response.

269 FEF neurons can be divided into three functional groups, related to whether their activity corresponds  
270 with visual stimuli, motor action, or both (Segraves and Goldberg, 1987). The Cope-Chambers model  
271 simplifies this categorisation using a single layer of 50 by 50 units representing the mean of all three  
272 groups. This layer therefore responds to both visual stimuli and the buildup of activity associated with  
273 motor (saccadic) action. The retina provides a persistent luminance signal into the FEF through the dorsal  
274 visual pathway (?) which is abbreviated in this model to a direct connection with delay.

275 The FEF provides input into the BG (Saint-Cyr et al., 1990) (to Str.D1, Str.D2 and STN) which, in turn,  
276 projects back to thalamus in a retinotopically organised way (Middleton and Strick, 2000; Lynch et al.,  
277 1994). In addition, the thalamic targets of this path are regions with strong reciprocal connections to the  
278 FEF (McFarland and Haber, 2002). In this way, the FEF forms channel-based loops through basal ganglia  
279 of the kind described above. Such circuits formed the basis of the model of Humphries and Gurney (2002).  
280 The thalamo-cortical loop may be thought of as an integrator of information, whose gain is modulated by  
281 inhibition from basal ganglia (Chambers et al., 2012; Cope and Gurney, 2011).

282 The superior colliculus (SC) is a sub-cortical nucleus which also plays a critical rôle in the generation  
283 of saccades (Hikosaka and Wurtz, 1983). Both FEF and SC have direct connections to the saccadic burst  
284 generator (SBG, see Sect. 2.3). If either is lesioned, the other can direct gaze, following a period of  
285 adjustement (Latto, 1977), albeit with some persistent deficits. The SC is also a direct target of output  
286 from the SNr (Jayaraman et al., 1977; Jiang et al., 2003) and can be influenced by the action selection  
287 mechanisms of the BG. In particular, it forms a loop with BG, but unlike its cortical counterpart in FEF, the  
288 input to basal ganglia comes via the thalamus [Fig 6(a), blue arrows].

289 While the SC has seven alternating cell- and fibre-rich layers (Wurtz and Albano, 1980), in most  
290 cases these are divided into the ‘superficial’ and ‘deep’ layers, which have significantly different response  
291 properties. Cells in the superficial layers, which receive input from the retina, are mainly visually responsive,  
292 with a preferred response to phasic events (luminance onsets and offsets) and movement on the visual  
293 field (Goldberg and Wurtz, 1972). In contrast, cells in the deep layers receive multi-modal input, including  
294 inhibitory input from the output structures of the BG (Jayaraman et al., 1977), and are directly involved  
295 in the generation of saccadic eye movements. Saccade related activity in the deep layers appears to  
296 generate saccades through ‘population coding’, with a weighted sum of activity across the retinotopy of SC  
297 determining the saccade target (Lee et al., 1988; van Opstal and van Gisbergen, 1990; Mays and Sparks,  
298 1980). The deep layers of SC receive input from the FEF in a topographic manner (Stanton et al., 1988a;  
299 Sommer and Wurtz, 2000).

300 The SC in the Cope-Chambers model is based on the the model described in Arai and Keller (2005), with  
301 the difference that the SNr input to the SC is generated by the BG model, rather than being hand-crafted.  
302 The SC model has a superficial and a deep layer, each of which is a 2-D array of 50 by 50 leaky integrator  
303 units arranged in the same retinotopic manner as the FEF (Wurtz and Albano, 1980).

304 The Cope-Chambers model incorporates a special connectivity pattern for visual input via cortical (FEF)  
305 and sub-cortical (thalamus) pathways. Due to the retinotopic mapping (Sect. 2.2.2), foveal luminances  
306 deliver a strong signal to the BG; roughly one third of the map is activated for the foveal targets used in  
307 this work (Fig. ??, red cross). This makes it virtually impossible for a peripheral target (Fig. ??, yellow  
308 cross) to win selection in the BG. Even if the peripheral target competed successfully to generate a  
309 saccade, this process would cause a significant delay, leading to latencies much larger than those observed  
310 experimentally. To overcome this problem, the Cope-Chambers model incorporates a mechanism in which  
311 the synaptic strength of connections between FEF, thalamus and striatum are reduced close to the fovea  
312 according to a shifted hyperbolic tangent. This connection is named ‘DecayingAtFovea’ in the SpineML  
313 implementation and follows a modified sigmoidal curve rather than tanh. In either case, the relation is  
314 ‘S-shaped’ and normalised to the range [0 1]. Far from the fovea (where the S-shaped curve has the value  
315  $\approx 1$ ), the connectivity pattern looks almost identical to a one-to-one connection.

316 Input to the Cope-Chambers model is provided through a simple retina model which directly samples  
317 from a larger ‘world array’ of pixel values. In the current model, the input for the retina is named ‘World’

318 and is the retinotopic projection [Fig. 7(b)] of the eye's field of view of the world [Fig. 7(a)] and the  
 319 luminant targets therein. The raw input in 'World' is fed into a population which adds noise, and then  
 320 via a delayed connection to FEF (the sustained retinal input path), to simulate processing through the  
 321 dorsal visual stream. It is also fed, without substantial delay, into two leaky integrator layers (Retina\_1  
 322 and Retina\_2) with different time constants, with the more slowly reacting layer (Retina\_2) inhibiting its  
 323 faster counterpart. The faster layer responds quickly to the appearance of a prolonged stimulus before it  
 324 is inhibited by the slow layer, forming a phasic response to stimulus onset. The mechanism ensures that  
 325 phasic rather than tonic responses arrive at the superficial SC from the retina.

326 The output of the Cope-Chambers model is determined by the activity in the SC\_deep population. The  
 327 activity in SC\_deep is first transformed from retinotopic co-ordinates into the Cartesian co-ordinates. The  
 328 centroid of the activity is then computed. The position of this centroid in the Cartesian frame determines  
 329 the saccadic end-point. The current model differs in that it does not compute a centroid, instead feeding the  
 330 SC\_deep activity into the saccadic burst generator.

331 The Cope-Chambers model was parameterised by tuning the model to perform a prosaccade task in which  
 332 a fixed luminance point is fixated by the model. After a fixed duration, the fixation point was extinguished  
 333 and a target point of fixed luminance was presented. The model was tuned so that the latency between the  
 334 presentation of the target and the initiation of an eye movement matched experimental data, while also  
 335 matching the electrophysiological evidence of activity in a variety of brain regions. The tuning of the BG  
 336 model attempted to preserve as closely as possible the weights used in the original paper. Further details on  
 337 the parameterisation of the Cope-Chambers model are in Cope et al. (2017).

### 338 2.2.1 Components

339 With the exceptions of the World and FEF\_add\_noise populations, each neural element represents an  
 340 activation; the activation is governed by a first order differential equation specified in the SpineML  
 341 component. In the brain model, there are six different components in use: LINlinear; LINret; LINexp;  
 342 D1MSN and D2MSN.

343 The LINlinear component governs the activation  $a$  with a first order leaky integrator differential equation:

$$\dot{a} = \frac{1}{\tau}(a_{in} - a) \quad (1)$$

344 where  $\tau$  is the time constant for the neural activation and  $a_{in}$  is the input to the neural element.  $a_{in}$  is  
 345 defined by an activation input and a shunting inhibition input according to:

$$a_{in} = A(1 - s_a) + \alpha R_N \quad (2)$$

346 Here,  $A$  is the activation input and  $s_a$  is the shunting inhibition state variable whose value is related to the  
 347 shunting input,  $S$  by

$$s_a = \begin{cases} S & S \leq 1 \\ 1 & S > 1 \end{cases} \quad (3)$$

348  $R_N$  is a random number drawn from a standard normal distribution ( $\sigma=1$ ,  $\mu=0$ ) and introduces noise to the  
 349 activation of the neural element, with the parameter  $\alpha$  controlling the noise amplitude.

350 The output,  $y$ , of LINlinear is related to the activation  $a$  by the piecewise linear transfer function

$$y(a) = \begin{cases} 0 & a < c \\ a - c & c \leq a \leq 1 + c \\ 1 & a > 1 + c \end{cases} \quad (4)$$

351 where  $c$  is a parameter defining the offset of the transfer function. If  $c < 0$ , then for zero activation ( $a = 0$ ),  
 352 the output will be positive. This simulates the effect of a neural population having tonic firing. If  $c > 0$   
 353 then the output will be zero until the activation exceeds  $c$ , simulating neurons which only fire when driven  
 354 by excitatory input. At this point, the naming scheme for the component becomes apparent; this is a Leaky  
 355 Integrator with a piecewise-linear transfer function.

356 The LINret component used for the retinal populations is similar to the LINlinear component, but with  
 357 no intrinsic noise and no shunting inhibitory input. It has a neural input which is identical to the activation  
 358 input  $A$ :

$$a_{in} = A \quad (5)$$

359 The LINexp component is a leaky integrator with an exponential transfer function. It shares the same  
 360 differential equation with LINlinear, but has a different input equation and a different output transfer  
 361 function. It has the following equation for the neural element input  $a_{in}$ :

$$a_{in} = [A + N(a - V_r^-)](1 - S) + 0.01R_N \quad (6)$$

362 where  $A$  is the activation input and  $N$  is an input which is modulated by  $V_r^-$ , a reversal potential, and  
 363  $a$ , the current activation of the element. These inputs are summed and then reduced by a factor which  
 364 is dependent on  $S$ , the shunting input. As in LINlinear,  $R_N$  introduces normally distributed noise to the  
 365 element.

366 The output,  $y$ , of the LINexp component is given by

$$y(a) = \begin{cases} e^a - 0.9 & e^a \leq 1 + 0.9 \\ 1 & e^a > 1 + 0.9 \end{cases} \quad (7)$$

367 This component is used in the subthalamic nucleus (STN) population, as it gives a more physiologically  
 368 accurate f-I behaviour (Wilson, 2004; Bevan and Wilson, 1999; Hallworth et al., 2003) which has been  
 369 shown to allow the mapping of the basal ganglia network architecture onto an optimal decision making  
 370 model (Bogacz and Gurney, 2007).

371 The D1MSN and D2MSN components are both leaky integrators, similar to LINlinear. They differ in  
 372 that they have no shunting inhibition. They are used to model medium spiny neuron (MSN) populations  
 373 in the striatum. As they model the fact that most MSN neurons fall into two groups; those expressing D1  
 374 dopamine receptors and those expressing D2 receptors, they have a dopamine parameter that modulates the  
 375 input activation, so that their equations for  $a_{in}$  are thus:

$$a_{in}^{D1} = (0.2 + d)A + 0.01R_N \quad (8)$$

$$a_{in}^{D2} = (1 - d)A + 0.01R_N \quad (9)$$

377 where  $d$  is the dopamine parameter. Varying dopamine from 0 to 1 enhances the activation in the D1 model,  
 378 whereas it decreases the activation of the D2 model elements, in line with experimental observations  
 379 (Harsing and Zigmond, 1997; Gonon, 1997). Note that the equation for  $a_{in}^{D1}$  differs from that used in  
 380 the Cope-Chambers model, for which the cortico-striatal weights are multiplied by  $(1 + d)$  rather than  
 381  $(0.2 + d)$ .

382 The equations given above are applied to each element in a population. The value of the activation  $A$  (and  
 383 where relevant, the shunting input,  $S$ ) is determined by summing the weighted inputs to the population:

$$A = \sum_i w_i^{act} x_i^{act} \quad (10)$$

384

$$S = \sum_i w_i^{sh} x_i^{sh} \quad (11)$$

385  $w_i^{act}$  and  $w_i^{sh}$  are, respectively, the weights of the  $i^{th}$  activation or shunting connection;  $x_i^{act}$  and  $x_i^{sh}$  are  
 386 the signals input to the activation and shunting connections.

### 387 2.2.2 Population activity and retinotopic mapping

388 Each population of 2500 neural elements was arranged in a 50 by 50 grid, with positions on the grid  
 389 representing a retinotopic mapping similar to that found empirically both in the superior colliculus (Ottos  
 390 et al., 1986) and in visual cortex (Schwartz, 1980) and assumed in this work to persist throughout the  
 391 oculomotor system.

392 In a retinotopic mapping, the Cartesian co-ordinates of the light-sensitive cells in the retina, whose density  
 393 varies with distance from the fovea, are transformed into the Cartesian co-ordinates of the correspondingly  
 394 active cells on the colliculus. The mapping ensures that an even density of cells can be maintained in the  
 395 colliculus, but ensures that a group of adjoining, active, retinal neurons will always activate an adjoining  
 396 group of neurons on the collicular surface.

397 The mapping turns out to resemble polar co-ordinates. That is, one axis of the collicular surface specifies  
 398 the eccentricity of a retinal location (how far it is from the fovea) and the second axis specifies the rotational  
 399 angle of the retinal location; we therefore use the convention of referring to the eccentricity axis on the  
 400 colliculus as  $r$  and the rotation axis as  $\phi$ .

401 The *cortical magnification factor*,  $M(r)$ , gives the relationship between the radial eccentricity  $r$  and the  
 402 retinal neural density. As in Cope et al. (2017), we use a first-order approximation of the form for  $M(r)$   
 403 given in Rovamo and Virsu (1979):

$$M(r) = \frac{M_f}{1 + \frac{r}{E_2}} \quad (12)$$

404 The foveal magnification,  $M_f$ , is the magnification of the most central region of the retina and has a value  
 405 in the human of about 7.8 mm/ $^\circ$  (Rovamo and Virsu, 1979).

406 In our model,  $M_f$  is related to  $W_{nfs}$ , the width of the retinotopic neural field,  $W_{fov}$ , the width of the  
 407 eye's field of view and  $E_2$ , the eccentricity at which the retinal density has halved by:

$$M_f = \frac{W_{nfs}}{E_2 \ln \left( \frac{W_{fov}}{2E_2} + 1 \right)} \quad (13)$$

408 Here,  $W_{nfs}$  is 50 (the side length of the 50x50 grid) and  $W_{fov}$  is set to  $61^\circ$ , a reduction from the  
 409 biophysically accurate  $150^\circ$  due to the small number of neurons in the retinotopic neural field.  $E_2$  is 2.5  
 410 (Cope et al., 2017; Slotnick et al., 2001).

411 The mapping from the retinotopic co-ordinates in the brain to rotational co-ordinates of the stimulus/  
 412 response was written down by Schwartz (1977, 1980) for measurements of striate cortex [visual  
 413 stimulus to electrophysiological response—Daniel and Whitteridge (1961); Talbot and Marshall (1941)]  
 414 and by Ottes et al. (1986) for superior colliculus data [electrophysiological SC stimulus to eye movement  
 415 response—Robinson (1972)]. We used the following statement of this mapping to introduce stimuli into  
 416 the ‘World’ input population of the brain model:

$$\phi = \frac{W_{nfs}}{2\pi} \arctan \left( \frac{\theta_y^t}{\theta_x^t} \right) \quad (14)$$

417

$$r = M_f E_2 \ln \left( \frac{1}{E_2} \sqrt{\theta_x^{t^2} + \theta_y^{t^2}} + 1 \right) \quad (15)$$

418 Note that we use  $r$  and  $\phi$  as the co-ordinates on the ‘collicular surface’. Schwartz uses  $r$  and  $\phi$  as the polar  
 419 coordinates of the retinal stimulus; Ottes et al. use  $r$  and  $\phi$  as polar coordinates for the eye movement  
 420 response; both use  $u$  and  $v$  as the Cartesian co-ordinates of the neural map. We use  $\theta_x^t$  and  $\theta_y^t$  to give Euler  
 421 rotations for the retinal target stimulus. Note also that the form of Eqns. 14 & 15 is slightly different from  
 422 that given in Ottes et al. (1986) because our  $\theta_x^t$  and  $\theta_y^t$  are not the polar co-ordinates used in that work.

423 The mapping encompasses the entire visual field; the value of  $\phi$  is allowed to vary from  $0^\circ$  to  $360^\circ$  along  
 424 its axis. Effectively, the two contralateral colliculi found in the biology are incorporated into a single,  
 425 square map, avoiding the need to carry out the kind of ‘colliculus gluing’ described in Tabareau et al.  
 426 (2007).

427 It is straightforward to show that the reverse mapping is given by:

$$\theta_x = E_2 \left( e^{\frac{r}{M_f E_2}} - 1 \right) \cdot \cos \left( \frac{2\pi\phi}{W_{nfs}} \right) \quad (16)$$

428

$$\theta_y = E_2 \left( e^{\frac{r}{M_f E_2}} - 1 \right) \cdot \sin \left( \frac{2\pi\phi}{W_{nfs}} \right) \quad (17)$$

429 where we have dropped the  $t$  superscript on  $\theta_x$  &  $\theta_y$ , as these equations transform a collicular location into  
 430 rotations of the eye.

431 Fig. 8 shows the result of the mapping for a view of two cross-shaped luminances. One cross illuminates  
 432 the fovea, which results in a large comb-shape of activity. The more peripheral cross produces (in FEF) an  
 433 indistinct object centred at a larger value of  $r$ .

### 434 2.2.3 Network

435 Briefly, the model consists of input from the World population (see Fig. 7, green population box)  
 436 producing activity in an ‘express’ pathway to superior colliculus (purple) and simultaneously in cortex,  
 437 represented here by the FEF population (grey boxes in Fig. 7). The express pathway causes short latency  
 438 activity in the superficial superior colliculus, which directly innervates the deeper layers of the superior  
 439 colliculus (SC\_deep). Activity in FEF generates firing in a thalamo-cortico-basal ganglia loop. The output

440 of the basal ganglia is the substantia nigra pars reticulata (SNr) which tonically inhibits SC\_deep. If a  
441 location of activity in FEF is able to dominate selection in the basal ganglia circuit, the corresponding  
442 location in SNr will dis-inhibit and activity will build up in SC\_deep encoding the saccade end point.

443 Connections shown in red are one to one connections; dark blue projections indicate a connectivity pattern  
444 which ‘fans out’ with a 2-D Gaussian kernel; lighter blue connections from the subthalamic nucleus (STN)  
445 to SNr and globus pallidus externum (GPe) are diffuse, all-to-all connections and projections coloured  
446 green are one-to-one connections that decay towards the fovea so that foveal activity in FEF does not  
447 swamp the basal ganglia which would prevent peripheral luminances from ever being selected. Note  
448 that SC\_deep contains two recurrent connections; one is excitatory, with a Gaussian kernel mapping and  
449 the other implements tecto-tectal inhibition, which increases the inhibition between activity in opposite  
450 hemispheres of the field of view (Gian G. Mascetti and Jorge R. Arriagada, 1981; Olivier et al., 2000)  
451 helping to resolve competition between saccades to the left and right. The tecto-tectal inhibitory connection  
452 is *not* present in the Cope-Chambers model. In all other respects the model is as described in Cope et al.  
453 (2017). We have not listed the parameters of the network in tabular form here, instead, the reader is referred  
454 to the SpineML declarative specification of the model from the link given in SUPPLEMENTAL DATA.  
455 The easiest way to access this information is by using SpineCreator.

### 456 2.3 Brainstem model

457 We implemented a saccadic burst generator (SBG) based on the connectivity outlined in Gancarz and  
458 Grossberg (1998). The SBG network for two of the model’s six channels is shown in Fig. 9. We use the  
459 word ‘channel’ to mean a set of populations of neurons which are involved in actuating a single extraocular  
460 muscle. SBG channels are arranged in pairs, actuating opposing muscles. There is one pair of channels  
461 which actuates the superior and inferior rectus muscles, causing vertical rotations of the eye in a roughly  
462 parasaggital plane (the eye moves up or down). Another pair actuates the lateral and medial rectus muscles,  
463 causing horizontal rotations of the eye. The third pair actuates the superior and inferior oblique muscles  
464 which contribute to vertical as well as oblique rotations. Activity from the output layer of superior colliculus  
465 (SC\_avg) is fed into each channel, which sums the activity it receives and processes it in populations each of  
466 a single neural element representing all the neurons in that population. Each channel of the SBG functions  
467 to create the motor neuron activations that are required to accelerate the eye in a particular direction, then  
468 hold the eye in its new position against the returning force generated by the elastic properties of the muscles.  
469 The required motor neuron activations are therefore a combination of features: a brief burst of increased  
470 activity that accelerates the eye; followed by a period of activity that is less than the burst firing rate but  
471 higher than the tonic rate that exists when the eye is at the centre. This holds the eye in its new position.

472 The SBG connectivity produces each of the these features separately, then sums them to create the desired  
473 ‘bump and tonic’ activation time series. The input to the first population in the SBG, the long-lead burst  
474 neurons (LLBNs), is conceived as originating from one of the deep layers of the superior colliculus. The  
475 activity of the LLBNs are passed to excitatory burst neurons (EBNs) which, in turn, inhibit the LLBNs via  
476 the activity of the inhibitory burst neurons (IBNs). This feedback loop has a transmission delay, which  
477 allows activity to build up in the EBNs before the inhibition is activated and the activity is then reduced  
478 again. This mechanism generates the ‘bump’.

479 The generation of the ‘tonic’ phase of the required time series is achieved simply by integrating the bump  
480 over time and multiplying by a some small gain factor. This is the function of the tonic neurons (TNs).  
481 The firing rate of the motor neuron defines the amount of force applied to the eye by that muscle. Thus,  
482 the integral of the ‘bump’ defines how far the eye moves in that channel’s direction. The gain and delay

483 parameters in the LLBN-EBN-IBN-LLBN feedback loop therefore have to be tuned such that the endpoint  
 484 of the saccade is reasonably accurate. Furthermore the restoring force generated by the elasticity of the  
 485 muscles is dependent on the radial distance. The value of the new tonic firing rate, after the ‘bump’ is  
 486 dependent on the end location of the eye. If the ratio between the EBN firing rate and the TN firing rate is  
 487 not exactly correct, the eye will drift away from the saccade endpoint after the saccade has been completed.  
 488 The EBN-TN connection strength is therefore tuned such that the TN firing rate yields a stable eye position  
 489 across a range of eye eccentricities.

490 The omnipause neurons (OPNs) are tonically active and inhibit the EBNs. The activity of the OPNs is  
 491 itself inhibited by activity in the LLBNs. The purpose of this arrangement is to ensure the eye does not  
 492 move in response to neural noise.

493 Each mean activity of all the neurons in each SBG population (except the TNs) is defined by a single  
 494 leaky integrator, first order differential equation.

$$\frac{da}{dt} = \frac{1}{\tau}(y - a) \quad (18)$$

495 where  $a$  is the activation of the nucleus, and  $\tau$  is the time constant of the nucleus.  $y$  is a piecewise linear  
 496 function of the weighted sum of inputs to the nucleus and is given by

$$y(IN) = \begin{cases} 0 & IN \leq b \\ IN - b & b \leq IN \leq 1 + b \\ 1 & IN \geq 1 + b \end{cases} \quad (19)$$

497 where  $b$  is the  $IN$  axis offset.  $IN$  is the weighted sum of inputs to the nucleus and is given by,

$$IN = \sum_m^M w_{mn} a_m \quad (20)$$

498 where  $a_m$  is the activation of the  $m^{th}$  afferent nucleus.  $w_{mn}$  is the connection strength between the  $m^{th}$   
 499 afferent nucleus and the current nucleus. The activity of the TNs are defined as

$$\frac{da}{dt} = \frac{1}{\tau} y \quad (21)$$

500 with an identical piecewise linear transfer function as the other SBG populations.

## 501 2.4 Biomechanical eye

502 The output signals of the brainstem are used to drive the biomechanical model. The latter is not only  
 503 used to get tangible feedback on the simulated saccades including motion trajectories, but adds one more  
 504 modelling dimension related to the inertial properties of the eye plant including muscle properties.

505 The biomechanical eye model, implemented using the OpenSim framework (Seth et al., 2011), is  
 506 anatomically represented by a sphere of uniform mass distribution. The diameter of the eye is 24 mm for  
 507 adults, with small variations between individuals; the mass of the eye is 7.5 grams. The eyeball is actuated  
 508 by six extraocular muscles (EOMs). The EOMs are arranged in three pairs forming a cone inside the orbit  
 509 with the apex being located inside the cranium in a tendonous ring called the annulus of Zinn. An important

510 feature of the oculomotor system which greatly affects its overall behavior is the existence of dynamic  
511 EOM pulleys. Their role is to guide the pivot point of the EOMs. In our model, a pulley for each EOM has  
512 been modeled by a point on the orbit whose location depends on the current eye orientation.

513 An illustration of the biomechanical eye model is given in Figure 1, while Figure 2 depicts the head  
514 model used in the proposed framework.

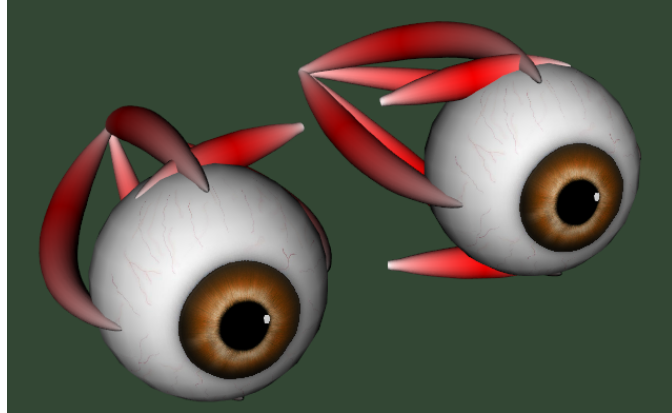


**Figure 1.** Example of the biomechanical eye model.

515 Two types of muscle models of different complexity are supported. The first models muscles using linear  
516 path actuators. This simplistic model of ideal muscles can be easily integrated with high level brain models.  
517 As described above the muscles are wrapped around the eye. The more complex model supported is based  
518 on the Thelen model (Thelen, 2003) that is also supported by OpenSim and implements Hill-type muscles.  
519 It includes realistic muscle wrapping geometric entities of the muscle fibers, while it accommodates for  
520 both activation and contraction dynamics. The dynamics of muscular forces can be split into: 1) The  
521 elasticity of the muscles. 2) A delay between the onset of the afferent excitatory signal and the actual  
522 muscle contraction, caused by the transmission time of the action potentials and by the necessary calcium  
523 release at the muscle fibres.

524 The force applied by EOMs is controlled by an excitatory signal supplied by motoneurons in the brainstem.  
525 The neural drive to produce a saccadic eye movement can be characterized by a pulse component to  
526 overcome the viscoelasticity of the orbital plant, a step component to stabilize the eye in the new position,  
527 and a slide component that models the gradual transition between the pulse and step.

528 Passive forces due to the fatty tissues inside the eye orbit also affect eye dynamics. Their role is critical in  
529 eliminating the influence of head and body movements. We incorporated a custom torque,  $t$ , which acts  
530 like a rotational spring-damper apparatus, resisting eyeball movements. It has elastic and viscous properties  
531 governed by  $t = -KR - CU$  where  $R$  is the eye's orientation and  $U$  is its angular velocity.  $K$  and  $C$  are  
532 constants. A fuller description of the biomechanical model can be found in Papapavlou and Moustakas  
533 (2014).

## 534 2.5 Model development framework

535 The Cope-Chambers model was originally developed to run on the BRAHMS model execution framework  
536 (Mitchinson et al., 2010; Mitchinson and James, 2015). To run a BRAHMS model, the researcher must  
537 develop *BRAHMS components* for the various neural elements. A BRAHMS component is a program-  
538 matically coded implementation of the behaviour of the component. It may have an arbitrary number of

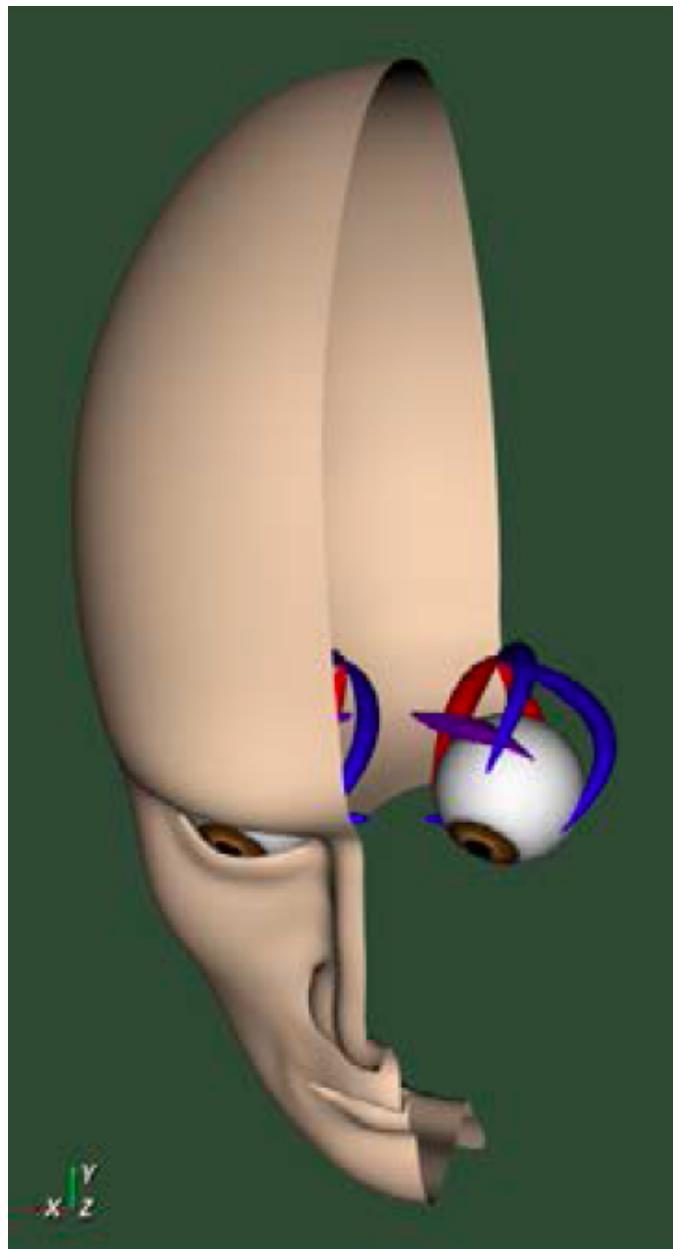


**Figure 2.** Example of the head model used.

539 inputs and outputs and may be written in C, C++, Python or MATLAB. The Cope-Chambers model's  
540 components were hand written in C++ and MATLAB. A BRAHMS *SystemML* file describes how the  
541 different components connect together and how data is passed between them (Mitchinson et al., 2010). The  
542 main BRAHMS program first reads the SystemML file, then dynamically loads all the required components  
543 before executing the system.

544 In the current work, the Cope-Chambers model was reproduced using the declarative SpineML markup  
545 language (Alex Cope and Paul Richmond, 2014; Richmond et al., 2014), with the help of the graphical  
546 SpineML model editing software called SpineCreator (Cope et al., 2015, 2016). SpineML, which is a  
547 development of the NineML specification (INCF Task Force on Multi-Scale Modeling, 2011), describes  
548 neural populations and their projections in a highly structured format in which neuron bodies, pre- and post-  
549 synapses are described in terms of *SpineML components*. These are similar to the components provided by

550 BRAHMS, but in this case, the components are an XML description of the functionality of the component,  
551 rather than a programmatic implementation, with one XML file per component. A SpineML *network layer*  
552 file then describes which components are used in the model, and how they are connected together. Finally,  
553 a number of SpineML *experiment layer* files specify how the model described in the network layer can be  
554 executed. In the experiment layer, the execution duration and timestep can be specified, along with input  
555 conditions, connection lesions and component parameter updates. A description of SpineML is given in  
556 Richmond et al. (2014); the definitive definition is found in the schemas (Cope et al., 2014). SpineCreator,  
557 in its rôle as a graphical editor for the SpineML format, was used to generate the SpineML files describing  
558 the model. It was also used to generate the diagrams of the model.

559 As a declarative format for model specification, SpineML is agnostic about how the model is executed. A  
560 number of simulation engines can be utilised, including DAMSON (Richmond, 2015), GeNN (Nowotny,  
561 2011; Nowotny et al., 2014) and BRAHMS (used here). The simulation engine incorporating BRAHMS is  
562 called SpineML\_2\_BRAHMS (Cope and James, 2015). SpineML\_2\_BRAHMS is a collection of XSLT  
563 stylesheets which first generate and compile C++ BRAHMS components from the SpineML component  
564 layer description files. SpineML\_2\_BRAHMS then uses the SpineML network and experiment layer files  
565 to generate a BRAHMS SystemML description of the model. Finally, SpineML\_2\_BRAHMS executes the  
566 model, now described entirely as a BRAHMS system, via a call to the BRAHMS binary. A number of  
567 additional hand-written components are present in SpineML\_2\_BRAHMS providing the inputs (constant  
568 inputs, time-varying inputs, etc) which the modeller specifies in the experiment layer.

569 In addition to the brain model components, all of which are code-generated using SpineML\_2\_BRAHMS as  
570 described above, two hand-written components are integrated into the model: The biomechanical eye model  
571 and a sensory input component. The sensory input component takes the eye's rotational state and the state  
572 of the experimental luminances and projects a retinotopic activity map into the brain model. Both of these  
573 BRAHMS components were hand-written in C++. To incorporate these components into the SpineML  
574 model, a SpineML\_2\_BRAHMS *external.xsl* file was used. The external.xsl file scheme for incorporating  
575 external BRAHMS components into a SpineML model was a new SpineML\_2\_BRAHMS feature motivated  
576 by the current work. Fig. 10 shows the workflow, in which the model specification files (blue box - a  
577 combination of SpineML files and C++ code), are processed (green box) into a BRAHMS system (red  
578 box).

579 Finally, numerical integration of the biomechanical eye model is based on the Kutta-Merson integration  
580 method.

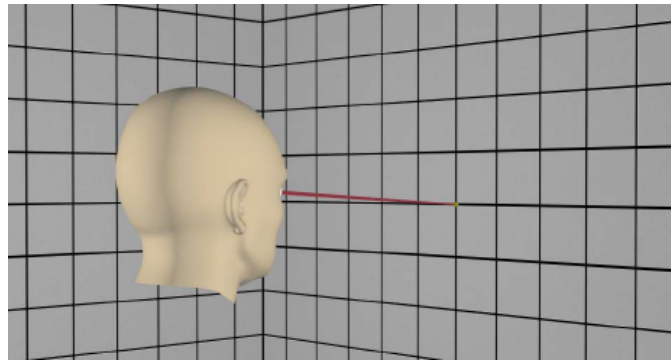


**Figure 3.** Example of the experimental set-up.

581     Figure 3 illustrates an example of the experimental set-up of the proposed framework, while Figures ??  
582 and 5 depict the developed eye oculomotor simulation system.

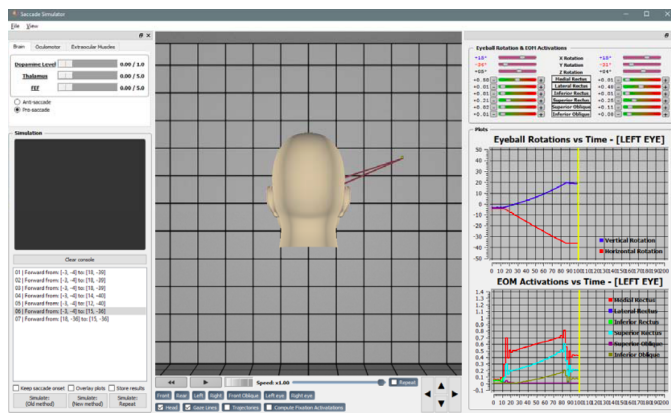


**Figure 5.** Example of use of the eye simulator system.

## 583 2.6 Integrating the models and closing the loop

584     The Cope-Chambers model closed its loop by passing the centroid of activity in SC\_deep (once it had  
585 surpassed a threshold) back to the code that controlled the world, which would then use this location to  
586 instantaneously change the model's view of the world. In our extended model, it was necessary to connect  
587 the output of the brain model back to its input via the saccadic burst generator model and the biomechanical  
588 eye. The resulting state of the eye, rather than the centroid of the superior colliculus, was used to compute  
589 the input to the brain, given the luminances visible in the world.

590     Thus, the information flow in the model is as follows: Luminances in the world have their locations  
591 computed in the eye's frame of reference, based on the rotational state of the eye. The locations of the  
592 luminances on the retina are transformed into a retinotopic co-ordinate system which determines the  
593 activity in the 'World' population (named to mean the 'world as the eye sees it', rather than the world  
594 frame of reference) which is the input for the brain model. The target luminance for a saccade is selected,  
595 as described earlier, via cortical and sub-cortical loops through the basal ganglia model and activity for  
596 the winning end-point builds up in the deep layer of superior colliculus. This activity excites activity  
597 in the correct proportions within the 6 channels of the saccadic burst generator whose output state, the  
598 motoneurons send a rate-code signal (normalised between 0 and 1) into the biomechanical eye model. The

599 rotational state of the eye model is fed back to participate in the computation of the retinotopic luminance  
 600 activity in ‘World’, completing the loop.

601 A number of studies have considered the form of the connection between the deeper layers of the superior  
 602 colliculus and the saccadic burst generator (Van Gisbergen et al., 1985; Ottes et al., 1986; Waitzman et al.,  
 603 1991; Groh, 2001; Arai et al., 1994; Goossens, 2006; Tabareau et al., 2007; van Opstal and Goossens, 2008;  
 604 Goossens and van Opstal, 2012), which has become known as the spatial temporal transform (STT). The  
 605 spatial aspect of the transform is thought to be implemented by a weight-mapping (Tabareau et al., 2007;  
 606 Arai et al., 1994) and we follow this idea. Arai and co-workers trained a 20x20 neural network model  
 607 of the superior colliculus to discover the weight map under the assumption of 2D Gaussian activation  
 608 profiles (Arai et al., 1994). The training approach of Arai et al. (1994) was not feasible in this study due to  
 609 the length of time required to run our model and its stochasticity, which meant multiple runs of the model  
 610 were necessary in order to generate output statistics. Tabareau et al. (2007) wrote down a theoretical form  
 611 of the weight map, which follows from the mapping of Ottes et al. (1986) and the assumption of invariant  
 612 2D Gaussian activity profiles in SC. As they found it closely resembles the results of Arai et al. (1994),  
 613 and it is a simple formulation, we considered it as the means to generate the six weight maps in our own  
 614 model. One barrier to the use of the weight map in Tabareau et al. (2007) was the Cope-Chambers model’s  
 615 violation of the *invariant integral hypothesis*. This states that the number of spikes emitted by a neural  
 616 element during a saccade (or in our model, the integral of the neuron’s output during the saccade) should  
 617 be a function only of its position within the hill of collicular activity. That is, for any time-dependent hill of  
 618 activity  $\mathcal{A}(\mathbf{z}, t)$  at  $\mathbf{z} = (r, \phi)$  on the collicular surface, the integrated activity  $A_{\mathbf{x}}$  in an element at a vector  $\mathbf{x}$   
 619 away from  $\mathbf{z}$  is

$$A_{\mathbf{x}} = \int_t \mathcal{A}(\mathbf{z} - \mathbf{x}, t) dt \quad (22)$$

620 which is invariant for all  $\mathbf{z}$ . However, the very mapping on which the Tabareau et al. (2007) result is based  
 621 leads to a very *variant* activity profile in the Cope-Chambers model. A luminance of a given size which  
 622 excites activity near to the fovea causes activity in a large number of neurons, whereas activity far from the  
 623 fovea excites a much smaller region. This effect is clearly demonstrated in Fig. 8 for equal sized targets  
 624 both on and distal from the fovea.

625 This led us to hypothesise that the retinotopic mapping be accompanied by an associated widening  
 626 projection field such that the hill of activity in superior colliculus is invariant with position on the collicular  
 627 surface. There are a number of locations in the system in which this widening projection field could exist.  
 628 It could be implemented in the projections between the retinal populations and the superficial layer of  
 629 SC along with the projection between the World and the FEF population. However, this would affect  
 630 activity within the basal ganglia of the model, contradicting a result in Cope et al. (2017) which explains  
 631 the ‘hockey stick’ profile for saccade latency as a function of saccade eccentricity. Instead, we suggest  
 632 that a widening projection field is encoded within the superior colliculus itself, a complex, multi-layered  
 633 structure which could quite plausibly support such a function. Indeed, such widening activity can be seen in  
 634 the stimulation experiments in Vokoun et al. (2010) and Vokoun et al. (2014). In Ghitani et al. (2014), from  
 635 the same research group, evidence is presented for an excitatory and widely projecting pathway from the  
 636 stratum griseum intermediale (equivalent to our SC\_deep) to the more superficial layers stratum opticum  
 637 and stratum griseum superficiale. Although this pathway is a ‘wide’ projecting field, the experiments do  
 638 not indicate whether the projection *widens* along the rostral-caudal axis of the SC. Bayguinov et al. (2015)  
 639 presents evidence for another projecting field within SC whose connectivity pattern *does* change along  
 640 the rostral-caudal axis. This projection is inhibitory in nature. Although neither of these results precisely

641 match the widening, excitatory projection field hypothesised here, they do indicate that such connection  
 642 patterns are plausible. Although in this work we do not model the SC in detail, we extended the model  
 643 with a third functional layer named SC\_deep2, shown in Fig. 11 (Cope-Chambers has only the two layers  
 644 SC\_sup and SC\_deep). We introduced a widening projection based on a Gaussian projection field whose  
 645 width,  $\sigma(r)$  varies in inverse proportion to the magnification factor,  $M(r)$ , given in Eq. 12 according to:

$$\sigma(r) = \frac{m_\sigma}{M(r)} - \frac{m_\sigma}{M^0} + \sigma_0 \quad r > r_0 \quad (23)$$

646  $m_\sigma$  is a scalar parameter which determines the ‘magnitude of the widening’.  $M^0$  is the ‘starting’ magni-  
 647 fication factor; within the foveal region ( $0 \leq r \leq r_0$ ), the projection field is not allowed to widen and  
 648 so

$$\sigma(r) = \sigma_0 \quad r \leq r_0 \quad (24)$$

649 which makes  $\sigma_0$  the width of the Gaussian projection field within the foveal region. (Note that the value  
 650 chosen for the width of the foveal region,  $r_0$  is not identical to the foveal shift parameter used in the  
 651 *DecayingAtFovea* projections into striatum.) The *Widening Gaussian* projection weight,  $w(r, d)$  is then  
 652 computed as:

$$w(r, d) = e^{-\frac{d^2}{2\sigma(r)^2}} \quad (25)$$

653 where  $d$  is the distance between the source and destination elements in the collicular plane.  $m_\sigma$  was set to  
 654 50,  $\sigma_0$  was 0.3,  $M^0$  was 12.43 and  $r_0$  was 20.

655 A further issue regarding the use of the theoretical weight map in Tabareau et al. (2007) was that it does  
 656 not consider the existence of the oblique extraocular muscles. There is evidence that only two dimensional  
 657 information is encoded in superior colliculus (Wurtz and Goldberg, 1972; Hepp et al., 1993; Van Opstal  
 658 et al., 1991), but the eye is actuated by six extraocular muscles. In order to find out a possible form for the  
 659 input to the oblique muscles we carried out a training process which depended on a centroid computation  
 660 in SC\_deep. For the four rectus muscles, the resulting weight maps resembled those found by Arai et al.  
 661 (1994). The trained maps for the oblique muscles had a form very close to those for the inferior and  
 662 superior rectus channels, but with a smaller magnitude. The inferior oblique map resembled the superior  
 663 rectus map and the superior oblique map resembled the inferior rectus. When parameterising the theoretical  
 664 weight maps, we set the inferior/superior oblique maps to be 1/10<sup>th</sup> of the superior/inferior rectus maps,  
 665 respectively. Interestingly, this suggests that there is a built-in synergy between the vertical and oblique  
 666 channels in the eye, although the results will show there is some systematic change in the oblique error  
 667 with saccade end-point location.

668 Tabareau et al. (2007) give a formulation for the weight maps in which it is possible to project both a  
 669 positive and a negative weight. In our model, all projections from SC\_deep are excitatory. This means that  
 670 each channel has a weight which follows the form:

$$w(r, \phi) = i e^{jr} \sin \left( \frac{2\pi\phi}{W_{nfs}} + k \right) \quad (26)$$

671 where  $i$ ,  $j$  and  $k$  are per-channel parameters for the weight maps.  $k$  is determined by the mapping. Only the  
 672 positive part of the sine is utilised.  $i$  and  $j$  are parameters to be found.

673 The saccadic burst generator model was originally conceived with the assumption of a step input, which  
 674 returns to zero activity at a suitable time to curtail the saccade and avoid staircase saccades (Gancarz and

675 Grossberg, 1998). In our model there is no such mechanism to reduce activity in SC\_deep, and elsewhere.  
676 Although a successful, accurate saccade towards a target luminance will remove the excitation which caused  
677 the activity in SC\_deep by bringing the target luminance within the masked, foveal region, the activity  
678 in SC decays too slowly to avoid additional saccadic movements. We found it necessary to hypothesise  
679 an inhibitory feedback mechanism from the SBG to the brain model. This is shown in Fig. 9, which  
680 indicates how the output from the inhibitory burst neurons (IBN) of the SBG model are used to feed back  
681 an inhibitory signal to the SC\_deep, thalamus and FEF populations in the brain model, resetting them ready  
682 for the next saccade.

683 The output signals from the six channels of the SBG were connected to the six motoneuron inputs of the  
684 biomechanical eye. The signal was normalised; a value of 1 meaning that all the motoneurons in the output  
685 population were firing at their maximum rate and the force exerted by the relevant extraocular muscle  
686 was maximal. Channels innervated extraocular muscles as follows: Up: superior rectus; Down: inferior  
687 rectus; Right: medial rectus; Left: lateral rectus; Z+: superior oblique; Z-: inferior oblique. Because the  
688 medial rectus induces a rightward rotation of the eye, our single virtual eye is a *left* eye. The OpenSim  
689 implementation of the biomechanical eye was ‘wrapped’ (in the software sense) in a BRAHMS component.  
690 This made it possible to integrate the OpenSim model into the BRAHMS framework. The wrapper ensured  
691 that the input and output signals were correctly transferred and, importantly, handled the disparity in the  
692 solver timesteps used in the OpenSim model (25 ms) and the neural model (1 ms). This was achieved by  
693 having the BRAHMS wrapper create a separate thread to run the OpenSim model. The BRAHMS wrapper  
694 component was called on each 1 ms timestep, receiving the instantaneous activations from the motoneurons  
695 in the SBG. These activations, and the current simulation time, were written into a shared memory area,  
696 accessible by the OpenSim thread. Running independently, the OpenSim thread would update its inputs  
697 (using the most recent values in the shared memory area) whenever the simulation time had increased  
698 by 25 ms. It would then recompute its outputs (the rotational state of the eye) and write these into the  
699 same shared memory. The BRAHMS wrapper would update its outputs whenever they were changed in  
700 the shared memory by the OpenSim thread. A direct connection of the six outputs of the BRAHMS eye  
701 model component to the six inputs of the worldDataMaker BRAHMS component was specified in the  
702 SpineML\_2\_BRAHMS external.xsl file.

703 The eye model outputs its rotational state at each timestep. The rotational state is used to compute  
704 the view of the world in the eye’s frame of reference. To simplify the calculation, the luminances exist  
705 on a spherical surface at the centre of which is the eye. A hand-coded BRAHMS component called  
706 worldDataMaker computes the projection of the luminances into the eye’s frame of reference and then  
707 converts this representation into a retinotopic map to pass into the brain model. The input to the brain  
708 model is thus able to change continuously, on every timestep, rather than in a step-wise fashion when a  
709 saccade occurs, as in the Cope-Chambers model.

710 In the worldDataMaker BRAHMS component, the rotational state of the eye was used to construct  
711 Euler rotation matrices which transformed between the world’s frame of reference and the eye’s frame of  
712 reference. The worldDataMaker component received a specification of the world luminances in a JSON  
713 file called luminances.json at the start of each simulation. luminances.json specified the position, shape,  
714 size, luminance, appearance time and disappearance time of an arbitrary number of luminances. With this  
715 information, the instantaneous rotational state of the eye and the parameters of the retinotopic transform, it  
716 was able to compute the instantaneous input to the brain model.

717 The final models, on which the results of this paper are based are named ‘TModel3’, ‘TModel4’ and  
718 ‘TModel5’. Descriptions of these, and earlier versions of the model can be found in the code repository  
719 given in SUPPLEMENTAL DATA.

### 3 RESULTS

#### 720 3.1 Weight maps

721 We found the best parameters for the exponential in Eq. 26 ( $i$  and  $j$ ) by a manual tuning process. After  
722 selecting values for  $i$  and  $j$  in either the horizontal or vertical/oblique channels, we ran the model 6 times  
723 at each of 8 target eccentricities ( $7^\circ$ – $14^\circ$ ) which were purely in the direction of the newly parameterised  
724 channel. The training saccades were produced as described below in Sect. 3.3, with the same fixation  
725 and target luminances (crosses of magnitude 0.2 and 0.3) but with the fixation offset and target onset  
726 occurring at 0.2 s. We measured the end-point of the saccade by detecting the location at which the saccade  
727 velocity had dropped below 0.005 of its peak. We iterated until the mean saccade endpoint plotted versus  
728 target was close to the ideal straight line—see Fig. 12(a) & (b). We applied the same parameters to both  
729 directions of each channel;  $i_{up} = i_{down} = 0.00195$ ,  $j_{up} = j_{down} = 0.075$ ,  $i_{left} = i_{right} = 0.0016$  and  
730  $j_{left} = j_{right} = 0.067$ .

731 The resulting weight maps (where the oblique maps are 1/10<sup>th</sup> of the vertical maps, as described earlier)  
732 are shown in Fig. 13. First, recall that the  $r$  axis of the neural surface corresponds to the amplitude of a  
733 saccade and the  $\phi$  axis indicates the polar direction of the saccade, as described in Sect. 2.2.2 and Fig. 8.  
734 Fig. 13(a) shows the weight map for the muscle which rotates the eye to the left. As we modelled a left  
735 eye, this actuates the lateral rectus muscle. The exponential rise of Eq. 26 is seen in the  $r$  direction; as  $r$   
736 increases, so the connection strength to the SBG channel rises exponentially. The connection strength is  
737 greatest along the centre line, for a value of  $\phi$  which corresponds to a purely leftward movement. Note that  
738  $\phi$  is presented in neural coordinates, and not in degrees or radians;  $1 \leq \phi \leq 50$  corresponds to a range of  
739  $0^\circ$  to  $360^\circ$ ;  $\phi = 38.5$  corresponds to movements left. The connections strength drops away sinusoidally  
740 as  $\phi$  moves away from the centre line at  $\phi = 38.5$ . In regions of the map for which there is no leftward  
741 movement, that is, in the half of the map which corresponds to any movement with a rightward component,  
742 the ‘left’ weight map is 0. Fig. 13(d) shows the weight map for rightward movements, actuating the medial  
743 rectus muscle of the eye. The line of maximum connection strength is along  $\phi = 13.5$ . The map is a mirror  
744 of Fig. 13(a), reflected about the line  $\phi = 26$ . The ‘left’ and ‘right’ weight maps are orthogonal; the non-zero  
745 region of the ‘left’ map is zero in the ‘right’ map and vice versa. Fig 13(b) & (d) show the weight maps  
746 for downward and upward eye movements; the ‘down’ map activates the SBG channel for the inferior  
747 rectus muscle, the ‘up’ map activates the superior rectus. Note that ‘down’ is not orthogonal either to ‘left’  
748 or ‘right’ because a saccade down and left is achieved by simultaneously activating both the lateral and  
749 inferior rectus muscles. However, the ‘up’ map is orthogonal to the ‘down’ map and spans the edges of  
750 the surface where  $\phi$  rolls over from 1 to 50. The line of maximum connection strength for the ‘up’ map is  
751 along  $\phi = 1$ ; for ‘down’  $\phi = 26$ . Based on the training described in Sect. 2.6, the maps driving the superior  
752 oblique (‘Z+’) and inferior oblique (‘Z-’) muscles were set to 1/10<sup>th</sup> of the ‘down’ and ‘up’ maps.

#### 753 3.2 Saccade accuracy

754 In Fig. 12, we showed the result of running the model to targets located on the principle axes, on which  
755 the model was trained. We then simulated single saccades to targets in one hemifield of the eye’s field of  
756 view, with eccentricities between  $6^\circ$  and  $14.5^\circ$ . As in the training, we ran the simulation 6 times for each

target,  $\theta^t = (\theta_x^t, \theta_y^t, 0)$  to obtain mean saccade end-points. Fig. 14 shows saccade accuracy results for an entire hemifield in the naïve model which passed the output of SC\_deep directly to SBG via the weight maps. The ratio of the magnitude of the error vector to the magnitude of the target vector is plotted using a colour map. This ratio is shown for the full, three dimensional error vector in Fig. 14(a) and for the  $x$ ,  $y$  and  $z$  components in Figs. 14(b)–(c). Inspection of Fig. 14(a) shows that the end-point error is minimal along the principle axes ( $\theta_x^t = 0$  or  $\theta_y^t = 0$ ) and maximal near the  $45^\circ$  oblique targets (blue lines) with the end point error as high as 80% of the programmed saccade magnitude. The  $x$  component error map in Fig. 14(b) shows the same trend, mirrored about the ‘Target X’ axis, whereas the  $y$  and  $z$  component errors are, relatively, much smaller. Because the  $x$  component of the error is clearly contributing to end point errors which would not be considered ‘on target’, especially for oblique saccades, we considered the effect of the non-uniform size of the hill of activity in SC\_deep.

In our model, the location, *size* and shape of activity in FEF, the basal ganglia, thalamus and superior colliculus is eccentricity dependent, in line with the retinotopic mapping stated by Ottes et al. (1986). More eccentric targets generate reduced activity, because fewer retinal neurons are excited far from the fovea. Cope et al. (2017) showed that this relationship can explain increased saccadic latencies for distal targets, resulting from reduced activity in the decision making circuitry of the basal ganglia. However, the notion that activity in superior colliculus is eccentricity-dependent conflicts with the result of Tabareau et al. (2007), who showed that an invariant hill of activity was required if this complex logarithmic weight mapping was to be used to drive a two-degree-of-freedom saccadic burst generator, and also with experimental findings, which do not show significant eccentricity dependence, at least in the burst layer (Anderson et al., 1998).

To bring our model in line with these results, whilst maintaining the eccentricity dependent activity in basal ganglia, we hypothesised that a ‘widening projection’ exists between two maps in superior colliculus. As described in Sect. 2.6, there is now experimental evidence for similar projections (Ghitani et al., 2014; Bayguinov et al., 2015) making this a plausible suggestion. Activities in one SC\_deep layer remains eccentricity-dependent, with loops back to thalamus and cortex and through basal ganglia. This activity is then fed through a projection, which applies a Gaussian projection field, whose width increases with increasing stimulus eccentricity according to Eq. 25. The activity in this second SC\_deep layer is then fed to the weight maps of the SBG. This model was called ‘TModel4’. TModel4 was parameterised such that its horizontal and vertical error was similar—so that its equivalent of Fig. 12 showed a similar sum of squares error.

Figs. 15(a)–(d) show the percentage errors for TModel4. First of all, note that the error magnitudes are much smaller. The mean errors are smaller for every axis. The largest errors produced by the model are approximately 15%, which are within the boundaries of what some authors have suggested would be regarded as an accurate saccade (McPeek and Keller, 2002; McPeek, 2006). The magnitude of the largest error vector is approximately  $1.5^\circ$ .

This result indicates that the exponential part of the Ottes et al. weight map from SC to the SBG cannot on its own compensate for the eccentricity-dependent size of the hill of activity. The introduction of a widening projection field substantially improves the mean accuracy of saccades across the field of view. We therefore suggest that the transformation between retinotopically mapped activity, and eccentricity-independent activity width occurs within the superior colliculus and works alongside a simple, monotonically increasing weight map between SC and the SBG channels.

### 798 3.3 Single saccades

799 Having finalised the model by setting the weight maps, we then proceeded to exercise the model  
800 (TModel4), starting with saccades to a single target; prosaccades. Fig. 16(a) shows 9 representative  
801 saccades to a single target luminance. Initially, the eye had rotational state  $\theta_x = \theta_y = \theta_z = 0$  with  
802 its fovea directed at a fixation luminance cross (span 6°, bar width 2°) of magnitude 0.2 (in arbitrary  
803 units). At a simulation time of 0.4 s, the fixation luminance was set to 0 and a target luminance cross  
804 of the same dimensions as the fixation but with magnitude 0.3 was illuminated at one of the 9 different  
805 locations, marked by crosses in Fig. 16(a). The resulting trajectories are plotted, with colour indicating the  
806 relationship between trajectories and target crosses. The approximate end-point error is visible in this figure,  
807 although the last point in each trajectory is the saccade position at 0.8 s and not the velocity-based end-point  
808 described above. Figs. 16(b) and (c) show the rotational components of the blue and red trajectories in  
809 Fig. 16(a) along with the target and fixation luminance values. Rotations are the eye's Euler rotational  
810 components in the world frame of reference.

### 811 3.4 Saccade Latencies

812 To verify that our implementation of the brain model has the same functionality as that reported in Cope  
813 et al. (2017), we investigated the effect on saccadic response times of: target eccentricity; and any gap  
814 or overlap between fixation off-time and target on-time. We showed that the full model reproduces the  
815 'hockey stick' shape shown in Fig. 7 of Cope et al. (2017) for horizontal [Fig. 17(a)], vertical [Fig. 17(b)]  
816 and oblique saccades (not shown). The latency increases with eccentricity far from the fovea because  
817 the retinotopic mapping reduces the activity in the basal ganglia for more eccentric targets (this effect is  
818 described in detail in Cope et al. (2017)). Closer to the fovea, the interaction between the foveal mask and  
819 the activity in FEF again leads to reduced input into the basal ganglia and an increased time to achieve  
820 disinhibition in SNr.

821 Fig. 17(c) shows latencies achieved when varying the time between fixation offset and target onset. This  
822 is termed the *gap condition*; and is represented by a scalar value which, if positive, refers to a gap between  
823 fixation offset and target onset, and when negative, signifies an overlap, with the fixation luminance  
824 persisting past the time at which the target is illuminated. A negative gap is also termed an *overlap*. Again,  
825 we verify the behaviour presented in Cope et al. (2017), explained as resulting from the inhibition of  
826 the cortico-thalamic loop by SNr. In the gap condition, when the fixation luminance is removed, activity  
827 in STN immediately begins to decay, allowing SNr activity to reduce and thereby reducing inhibition  
828 on thalamus, allowing the target luminance to build up quickly in FEF, thalamus and through the basal  
829 ganglia's striatum and SNr. The shape of the curves in Fig. 17(c) matches the results in Cope et al. (2017)  
830 for target luminances of 1 and 0.6; for overlaps longer than 100 ms (gap < -100 ms), the latency becomes  
831 constant; the saccade is programmed whilst the fixation is present, with the target luminance inducing  
832 sufficient activity in striatum to 'break through' the SNr inhibition caused by the fixation. If the target  
833 luminance is reduced to 0.3, the balance is altered in favour of the fixation and the latency vs. gap becomes  
834 approximately linear and equal to the overlap time plus around 100 ms.

835 Fig. 17(d) shows the effect of the dopamine parameter on saccade latencies in gap, step and overlap  
836 conditions. In general, the effect of decreasing the dopamine parameter was a smooth, monotonic and  
837 undramatic increase in saccade latency. However, the data for the overlap condition with a target luminance  
838 which was 3 times as bright as the fixation luminance was more interesting. Here we see a transition around  
839 a dopamine value of 0.7. Below this value, the basal ganglia is not able to select the target luminance until  
840 the fixation is removed, reducing the excitatory drive from STN to SNr, and consequently the inhibition

841 from SNr to the thalamo-cortical loop. For the target luminance 0.6, 0.7 dopamine allows the basal ganglia  
842 to select sufficiently well so that the target can build up in the thalamo-cortical loop, in spite of the fixation  
843 overlap.

844 The relationship between latency and the target luminance is given in Fig. 17(e). This shows latency for a  
845 100 ms gap, step and 100 ms overlap conditions for a given fixation luminance of 0.2, and a horizontally  
846 located target at  $\theta_y^t = -10^\circ$ . For the gap condition, we see very short latencies for luminances of about  
847 0.75 and above. Finally, the activity driving these express saccades is initiated by high firing rates in the  
848 superficial layer of SC (SCs), which then drives activity in thalamus and through the basal ganglia. A  
849 gradual transition from express saccades to reflexive saccades is observed as the contribution of the SCs  
850 becomes weaker and the drive from FEF into the thalamo-cortical loop becomes necessary to elicit a  
851 saccade. A similar gradual transition, albeit for higher latencies is seen for the step condition. At higher  
852 target luminances, the SCs has a greater effect on the activity in the thalamo-cortical loop. However, the  
853 activity in STN caused by the fixation luminance increases the latency at all luminance values compared  
854 with the gap condition. The overlap condition leads to increased latencies for luminances below 2.5, but  
855 meets the step condition above this value, at which the 0.2 fixation luminance appears to have a negligible  
856 effect on the system.

### 857 3.5 Saccade sequences

858 We now present results derived from the fully parameterised and integrated model; where we took  
859 advantage of the fact that it is a closed loop system. This allowed us to present sequences of target  
860 luminances and allow the model to direct its fovea at the most salient target.

#### 861 3.5.1 Out & return

862 We investigated the behaviour of the model for saccade sequences. In one experiment, we illuminated  
863 a fixation cross from 0 s until 0.4 s, followed by a target at  $(0, -10^\circ)$  from 0.4 s until 0.8 s. Finally, the  
864 fixation was again shown from 0.8 s until the end of the simulation at 2 s. This induced a saccade to a  
865  $10^\circ$  eccentricity, followed by a return saccade back to the null point. We noticed some irregularities in  
866 the return saccades, which were accurate, but had a significant overshoot. More perplexingly, if the target  
867 was switched repeatedly between  $0^\circ$  and  $10^\circ$ , second and subsequent outward saccades also showed this  
868 overshoot. We found that the cause of these irregularities was the lack (in ‘TModel4’) of any mechanism to  
869 reset the tonic neurons in the SBG after the first saccade. This resulted in TN activity in the left channel  
870 and also in the right channel. Interestingly, this ensured that, at least for a few, consecutive out-and-return  
871 saccades, the saccade accuracy was accidentally relatively good, with trajectories resembling experimental  
872 data (Bahill and Stark (1979), p. 6). Had the return accuracy not been so accurate, we may have noticed the  
873 lack of a tonic neuron reset mechanism and corrected this oversight earlier. Such a mechanism is indeed  
874 proposed and included in the connectivity of the Gancarz and Grossberg (1998) model. We implemented  
875 this feature by adding an additional inhibitory input to the ‘integrator’ component of TModel4, driven  
876 by the contralateral EBN population, naming the new model ‘TModel5’. Now, when the eye is directed  
877 towards an eccentric target which is then exchanged with a target at the null point, the EBN activity toward  
878 the null point will tend to extinguish the TN activity which was holding the eye at the eccentric position.  
879 We verified that none of the single saccade results were affected by this modification.

880 Fig. 18 shows the outward and return trajectories produced by the experiment with the TN reset mecha-  
881 nism. Panel (a) shows the  $x$  and  $y$  rotation trajectory; panel (b) shows individual rotational components of  
882 the eye. Fig. 18(c) shows out and return trajectories for three other saccade targets; horizontal, vertical and

883 oblique. The trajectories have characteristic shapes and also show some stochastic variation caused by the  
884 noise in the model [see dashed trajectories in Fig. 18(a)].

885 The return trajectories (magenta lines) showed a distinctly different form from the outward trajectories.  
886 They overshot their destination (the null point) significantly. This resulted from the removal of the TN  
887 activity which was holding the eye at the eccentric target location. Removal of this activity, and thus the  
888 static force exerted by the corresponding extraocular muscle, meant that the eye was subject both to a new  
889 muscular force towards the null point *alongside* the restorative spring force of the lengthened rectus muscle.  
890 This stands as a shortcoming of the model.

891 **3.5.2 Double steps**

892 In another experiment, we probed the response of the model to double step stimuli of the type described  
893 in Becker and Jürgens (1979). In that work, the response of human subjects was investigated when shown  
894 stimuli at 15° and 30° eccentricity with variable delay between the stimuli. If the smaller eccentricity  
895 stimulus was shown first, followed by the more distal on the same side of the field of view, this was called  
896 a ‘staircase’ presentation. We carried out a ‘staircase’ presentation, shown in Fig. 19, where our small  
897 eccentricity luminance was at 8° and our more distal luminance was at 12° (both to the right of centre). We  
898 found that there was a critical time delay between the luminances of about 30 ms. If they were presented  
899 with a delay smaller than this value, then a single, slightly hypermetric saccade was made. This response  
900 type is called a *final angle response*. A delay greater than 30 ms between the stimuli would lead to double  
901 step saccades (a so-called *initial angle response*), with the first saccade arriving at 8° (though with greater  
902 variability than normal), and a second saccade being made to a location hypometric of 12° after a pause  
903 of about 240 ms. Fig. 19(a) shows the mean trajectories from 5 simulations of the staircase doublestep  
904 presentation alongside the result for a single saccade to the final angle of 12°. Dash-dot lines show ±1  
905 standard deviation about the mean. The corresponding trajectories are shown in Fig. 19(b).

906 Inspection of the activity maps in FEF and SC\_deep (not shown) indicates that when the 8° target  
907 is illuminated for 30 ms or more, the activity associated with this target angle is able to dominate the  
908 activity, hence the execution of a reasonably accurate saccade. The inhibitory feedback from the SBG then  
909 extinguishes activity in FEF, thalamus and SC, which means that a full 200 ms or more is required to allow  
910 activity in these populations to build up again in order to make the smaller saccade from 8° to 12°. This is  
911 in contrast to experimental findings in which the corrective second saccade is often executed *more quickly*  
912 than if it were programmed on its own (Becker and Jürgens, 1979).

## 4 DISCUSSION

913 The aim of this study was to demonstrate the importance of modelling neurological systems *in concert with*  
914 the biomechanical systems with which they have evolved in parallel. We hypothesised that by combining  
915 existing neurophysiological models with an accurate model of a musculo-skeletal system, and then ‘closing  
916 the loop’ by allowing the movements of the virtual muscles to modulate sensory feedback to the brain model,  
917 shortcomings in the constituent models would be revealed, leading to new knowledge. To demonstrate the  
918 validity of this hypothesis, we built an integrated model and then identified the modifications which were  
919 necessary to give it the ability to make accurate movements under one type of stimulus. We then examined  
920 its behaviour with other stimuli.

921 We chose the oculomotor model as a basis for this study because it has only three degrees of freedom,  
922 making it one of the simplest musculo-skeletal systems. Furthermore, eye movements fall into several

923 well-defined categories, each being controlled by separate brain circuits, we were therefore justified in  
924 modelling a system which produced only saccadic eye movements. Nevertheless, we are aware that we  
925 did not create a complete model of the system; no treatment of the cerebellum was attempted, justified  
926 because cerebellum appears to have only a minor effect on saccade accuracy (Dean and Porritt, 2008),  
927 probably correcting for slow to medium timescale changes in the physical dynamics of the eyeball (Dean  
928 et al., 1994).

929 To summarise our model integration: We combined the Cope-Chambers model (Cope et al., 2017) with a  
930 saccadic burst generator model based on the work of Gancarz and Grossberg (1998), using this to drive the  
931 input of a new biomechanical eye model. To achieve the spatial transformation from the retinotopic maps of  
932 the Cope-Chambers model to the six ‘muscle channel’ inputs for the saccadic burst generator, we used the  
933 mapping of Ottes et al. (1986) to produce parameterised weight maps along with an empirically discovered  
934 synergy for the torsional weight maps. We introduced an additional transformation to the brain model to  
935 achieve invariant sized hills of activity in superior colliculus to fulfil the invariant integral hypothesis of  
936 Tabareau et al. (2007). We closed the loop using a software component which transformed a view of a  
937 world containing luminous cross shapes into the eye’s frame of reference, given its instantaneous rotational  
938 state. This component also computed the inverse of the mapping from Ottes et al. (1986) to project the  
939 view retinotopically into the brain model. This paper serves to describe how we achieved the integration in  
940 order to test our hypothesis, and we intend that the material and methods section, along with the model  
941 code itself, will help others to carry out similar studies. However, we wish to devote the majority of this  
942 discussion to what can be learned from an integrated model of a combined brain and biomechanical system,  
943 using our oculomotor system as an example.

944 Our integration approach revealed three ways in which this model fails to provide a full understanding  
945 of the saccadic system. In each case, the issue is made clear *as a result of the integration*. This is not to  
946 say that other approaches may not also reveal shortcomings; we will see that one of our cases has been  
947 independently identified (Groh, 2011).

#### 948 4.1 The need for a widening projection field

949 The original combination of the Cope-Chambers model with the theoretical weight maps of Ottes et al.  
950 (1986) and Tabareau et al. (2007) resulted in a model which was able to produce accurate saccades only  
951 along the principle rotational axes (Fig. 14). Thus, *the integration of the models* suggested that an additional  
952 layer was required to achieve accurate saccades for oblique, as well as for horizontal and vertical saccades.  
953 Although the *need* for an invariant integral is discussed in Tabareau et al. (2007) as resulting from their  
954 theoretical study, the mechanism by which such an invariant Gaussian hill is generated is not. By combining  
955 the models, we were forced to consider this mechanism, and hypothesised that a widening projection field  
956 would be a candidate mechanism. The results of Fig. 15 indicate that a substantial improvement in accuracy  
957 is indeed achieved by this new mechanism.

#### 958 4.2 Saccades from non-null starting positions

959 The implementation of a biophysically accurate model of the eye, and the closed-loop nature of the  
960 model makes it very natural to consider how the model will behave making saccades from arbitrary starting  
961 positions, or how it would respond to a sequence of stimuli. This was the motivation for the out-and-return  
962 experiment (Fig. 18) as well as for the double step experiment (Fig. 19). We found that return saccades were  
963 substantially affected by the biomechanics of the eye, as the brain and brainstem model had no mechanism  
964 to account for the position-dependent restoring forces applied by the eye. This question has been addressed

965 by other authors; Groh (2011) investigates the effect of initial eye position on stimulated saccades and finds  
966 a need for the signal in superior colliculus to be modulated by an eye position signal. Ling et al. (2007)  
967 shows the existence of a position dependent firing rate offset in abducens neurons. Though we will not  
968 speculate here on the mechanism by which return saccades may be made accurate whilst also resetting  
969 the activity of tonic neurons in the SBG, it is interesting that in the model in which we omitted to reset  
970 TN activity (TModel4), we obtained relatively accurate out-and-return saccades which closely resembled  
971 experimental data. We suggest that residual activity in TN populations may offer an explanation for how  
972 the restorative force exerted by the elastic oculomotor muscles is compensated for. A comparison of this  
973 idea with that of Groh (2011) (that there is a modulation, from a brainstem signal, of the SC readout) would  
974 make a subject for a future study. Although these existing studies have highlighted this issue, the inaccurate  
975 return saccades which the model makes from eccentric starting positions provide a clear example of the  
976 way in which integrating known models into a closed-loop system can highlight deficiencies in the model.

### 977 4.3 Inhibitory feedback from saccadic burst generator to brain

978 The third issue raised by the integration of the component models of the saccadic system has, like  
979 the return saccades, to do with resetting activity. In this case, rather than the reset of activity in the TN  
980 population in the brainstem, it is the question of how the activity in the *brain* model should be reset after  
981 each saccade. When a target luminance is projected onto the World population in the model, this induces  
982 activity which ‘reverberates’ in loops through FEF, basal ganglia, SC and thalamus. The brainstem contains  
983 a mechanism to limit the timescale of a saccade (inhibitory feedback from EBN, via IBN to LLBN; see  
984 Fig. 9). However, if the activity in SC is not reset, then following the completion of the first saccade, a  
985 series of subsequent ‘staircase’ saccades will be executed. There needs to be a mechanism to extinguish  
986 activity in SC, but also in FEF and thalamus, as activity in either of these populations can build up and  
987 eventually cause repeat activity in SC and another saccade. We added hypothetical inhibitory feedback  
988 connections to our model, such that the IBN populations in the SBG would inhibit activity in FEF, thalamus  
989 and SC\_deep (Fig. 9), preventing the occurrence of staircase saccades.

990 An examination of the behaviour of the model when presented with ‘double-step stimuli’ reveals a  
991 problem with this scheme. We found that when double-step stimuli were presented (where an initial target  
992 at 8° was replaced with a 12° target after 30 or 40 ms) and a double saccade was made [Fig. 19(a), black  
993 lines] the second saccade latency was *longer* even than the initial saccade. This contrasts with Becker and  
994 Jürgens (1979) who find that second, corrective saccades occur with *shorter* latencies. This suggests that  
995 the inhibitory reset signal implemented in this model is too strong or has the wrong timescales. This issue  
996 highlights the fact that connections *between* component models are quite as important as the connections  
997 within each model.

### 998 4.4 Concluding remarks

999 The omission of the cerebellum will not have escaped the reader’s notice. Whilst many of the nuclei  
1000 known to be involved in the production of saccadic eye movements are incorporated within the model,  
1001 the cerebellum is not. The cerebellum is known to play an important rôle in saccade programming (Dean  
1002 et al., 1994; Schweighofer et al., 1996; Quaia et al., 2000; Kleine, 2003). It may be able to completely  
1003 replace the functionality of the colliculus when lesioned (Aizawa and Wurtz, 1998; Lefèvre et al., 1998).  
1004 However, this rôle is typically considered to be one of accuracy tuning (Barash et al., 1999; Dean et al.,  
1005 1994); operating as an additive model. Furthermore, saccades made by individuals with cerebellar ataxias  
1006 perform with only moderate loss of saccade accuracy (Barash et al., 1999; Federighi et al., 2011). Because  
1007 we did not address learning in our model, and because our aim was to demonstrate the utility of integrating

1008 brain with biomechanics in order to highlight deficiencies, we considered the omission of the cerebellar  
1009 nuclei acceptable in the present work.

1010 We have not addressed the question of saccade duration in this paper. Saccade duration is of interest in  
1011 models which produce two (or three) dimensional saccades, because the dynamics of a saccade follow well  
1012 known relationships with the saccade eccentricity, regardless of the saccade angle. This causes a problem for  
1013 models (such as the present one) for which some of the dynamic behaviour is generated within orthogonal  
1014 components. For example, saccade duration increases with target eccentricity. A 10° eccentricity oblique  
1015 (45° up and right) saccade is composed (approximately) of a 7° upwards component and a 7° rightwards  
1016 component. If the component based model is responsible for the dynamics, then the 10° oblique saccade  
1017 would be expected to have the dynamics of a 7° up or 7° right saccade. This is not found in practice, and  
1018 the components are said to have been stretched, hence the name for this effect ‘component stretching’. The  
1019 Gancarz and Grossberg (1998) model is reported to take account of the component stretching effect via  
1020 the OPN neuron population. We did not find this effect in our implementation of the model; the duration  
1021 of oblique saccades at a given eccentricity was always substantially different from the duration of the  
1022 corresponding purely vertical or horizontal saccade. Because there is a somewhat complicated interplay  
1023 between the dynamics of the superior colliculus driving the dynamic system of the SBG, we feel this is  
1024 outside the scope of the current work and a subject for a future paper.

1025 This work represents a step forward in the modelling of neuromuscular systems, not because it sig-  
1026 nificantly advances any of the constituent models, but because it *integrates* the models into a complete,  
1027 *behaving* system. This is not the first integrated brain model composed of separately developed components.  
1028 The works of N’Guyen et al. (2014) and Thurat et al. (2015) are both based on an example of a brain model  
1029 which drives a simple, second order model of the eye. DeWolf et al. (2016) describes a reach model which  
1030 integrates models of cortex and cerebellum to drive a two degree-of-freedom arm model. Both of these  
1031 example systems nevertheless operate using ‘curated’ inputs supplied by the modeller.

1032 In contrast, the current work allows the state of the system to determine the input delivered to the model.  
1033 The modeller only curates the state of the world at each time point, but the actual input to the model  
1034 depends on the eye’s rotational state. This is, to our knowledge, the first model which integrates the brain  
1035 with an accurate biophysical system and closes the loop in this way, enabling the system to reproduce  
1036 behaviour. As such, it offers a platform for testing more complex saccadic behaviour such as antisaccades  
1037 or saccades in the presence of distractor stimuli. We believe that by building closed loop systems which  
1038 express behaviour, we, and others will develop a new field of *computational neurobehaviour*, which will  
1039 share themes from neuroscience, artificial intelligence, decision science and embodied robotics.

## DISCLOSURE/CONFLICT-OF-INTEREST STATEMENT

1040 The authors declare that the research was conducted in the absence of any commercial or financial  
1041 relationships that could be construed as a potential conflict of interest.

## AUTHOR CONTRIBUTIONS

1042 SJ, AB and AC implemented existing parts of the model in SpineML. AB developed the saccade generator  
1043 brainstem model. SJ performed the technical and scientific integration of the biomechanical eye. CP and  
1044 KM developed the biomechanical eye model. SJ wrote the manuscript; SA, AB, KG and KM contributed  
1045 to the manuscript. KG conceived the project.

## ACKNOWLEDGEMENTS

1046 Funding: European Union FP7 Grant 610391 ‘NoTremor’.

## SUPPLEMENTAL DATA

1047 The model specification, results and all code required to reproduce the results of this work are available at:  
1048 [https://github.com/ABRG-Models/OMM\\_NeuroMuscular](https://github.com/ABRG-Models/OMM_NeuroMuscular)

## REFERENCES

- 1049 Aizawa, H. and Wurtz, R. H. (1998). Reversible inactivation of monkey superior colliculus. I. Curvature of  
1050 saccadic trajectory. *Journal of neurophysiology* 79, 2082–2096
- 1051 Alex Cope and Paul Richmond (2014). SpineML. RRID: SCR\_015641
- 1052 Anderson, R. W., Keller, E. L., Gandhi, N. J., and Das, S. (1998). Two-dimensional saccade-related  
1053 population activity in superior colliculus in monkey. *Journal of Neurophysiology* 80, 798–817
- 1054 Arai, K., Keller, E., and Edelman, J. (1994). Two-dimensional neural network model of the primate  
1055 saccadic system. *Neural Networks* 7, 1115. doi:10.1016/S0893-6080(05)80162-5
- 1056 Arai, K. and Keller, E. L. (2005). A model of the saccade-generating system that accounts for trajectory  
1057 variations produced by competing visual stimuli. *Biological cybernetics* 92, 21–37. doi:10.1007/  
1058 s00422-004-0526-y
- 1059 Bahill, A. T. and Stark, L. (1979). The trajectories of saccadic eye movements. *Scientific American* 240,  
1060 108–117
- 1061 Barash, S., Melikyan, A., Sivakov, A., Zhang, M., Glickstein, M., and Thier, P. (1999). Saccadic dysmetria  
1062 and adaptation after lesions of the cerebellar cortex. *Journal of Neuroscience* 19, 10931–10939
- 1063 Bayguinov, P. O., Ghitani, N., Jackson, M. B., and Basso, M. A. (2015). A Hard-Wired Priority Map  
1064 in the Superior Colliculus Shaped by Asymmetric Inhibitory Circuitry. *Journal of Neurophysiology*  
1065 doi:10.1152/jn.00144.2015
- 1066 Becker, W. and Jürgens, R. (1979). An analysis of the saccadic system by means of double step stimuli.  
1067 *Vision Research* 19, 967–983. doi:10.1016/0042-6989(79)90222-0
- 1068 Bevan, M. D. and Wilson, C. J. (1999). Mechanisms underlying spontaneous oscillation and rhythmic  
1069 firing in rat subthalamic neurons. *The Journal of neuroscience : the official journal of the Society for  
1070 Neuroscience* 19, 7617–28
- 1071 Blenkinsop, A., Anderson, S., and Gurney, K. (2017). Frequency and function in the basal ganglia: the  
1072 origins of beta and gamma band activity. *The Journal of Physiology* doi:10.1113/JP273760
- 1073 Bogacz, R. and Gurney, K. (2007). The basal ganglia and cortex implement optimal decision making  
1074 between alternative actions. *Neural Computation* 19, 442–477. doi:10.1162/neco.2007.19.2.442
- 1075 Bolam, J., Hanley, J., Booth, P., and Bevan, M. (2000). Synaptic organisation of the basal ganglia. *Journal  
1076 of Anatomy* 196, 527–542
- 1077 Brown, P., Oliviero, A., Mazzone, P., Insola, A., Tonali, P., and Di Lazzaro, V. (2001). Dopamine  
1078 Dependency of Oscillations between Subthalamic Nucleus and Pallidum in Parkinson’s Disease. *J.  
1079 Neurosci.* 21, 1033–1038
- 1080 Bruce, C. J. and Goldberg, M. E. (1985). Primate frontal eye fields. I. Single neurons discharging before  
1081 saccades. *Journal of Neurophysiology* 53, 603–635
- 1082 Casteau, S. and Vitu, F. (2012). On the effect of remote and proximal distractors on saccadic behavior: A  
1083 challenge to neural-field models. *Journal of vision* 12, 14

- 1084 Chambers, J. M., Gurney, K., Humphries, M., and Prescott, A. (2012). Mechanisms of choice in the  
1085 primate brain: a quick look at positive feedback. In *Modelling Natural Action Selection* (Cambridge  
1086 University Press). 390–420
- 1087 Chen, L. L. and Wise, S. P. (1995). Supplementary eye field contrasted with the frontal eye field during  
1088 acquisition of conditional oculomotor associations. *Journal of Neurophysiology* 73, 1122–1134
- 1089 Chevalier, G. and Deniau, J. M. (1990). Disinhibition as a basic process in the expression of striatal  
1090 functions. *Trends in Neurosciences* 13, 277–280
- 1091 Cohen, J. Y., Heitz, R. P., Woodman, G. F., and Schall, J. D. (2009). Neural basis of the set-size effect in  
1092 frontal eye field: timing of attention during visual search. *Journal of Neurophysiology* 101, 1699–1704.  
1093 doi:10.1152/jn.00035.2009
- 1094 Cope, A., Chambers, J. M., Prescott, T. J., and Gurney, K. N. (2017). Basal Ganglia Control Of  
1095 Reflexive Saccades: A Computational Model Integrating Physiology Anatomy And Behaviour. *bioRxiv*  
1096 doi:10.1101/135251
- 1097 Cope, A. and Gurney, K. N. (2011). A biologically based model of active vision. In *Proceedings of  
1098 AISB'11 - Architectures for Active Vision*, eds. S. O'Keefe, Kazakov, D., and Tsoukas, D. (York, UK),  
1099 13–20
- 1100 Cope, A. J. and James, S. S. (2015). SpineML\_2\_brahms. RRID: SCR\_015640
- 1101 Cope, A. J., Richmond, P., and Allerton, D. (2014). The SpineML toolchain: enabling computational neu-  
1102 roscience through flexible tools for creating, sharing, and simulating neural models. *BMC Neuroscience*  
1103 15, P224
- 1104 Cope, A. J., Richmond, P., and James, S. S. (2015). SpineCreator. RRID: SCR\_015637
- 1105 Cope, A. J., Richmond, P., James, S. S., Gurney, K., and Allerton, D. J. (2016). SpineCreator: a  
1106 Graphical User Interface for the Creation of Layered Neural Models. *Neuroinformatics* doi:10.1007/  
1107 s12021-016-9311-z
- 1108 Daniel, P. M. and Whitteridge, D. (1961). The representation of the visual field on the cerebral cortex in  
1109 monkeys. *The Journal of Physiology* 159, 203–221. doi:10.1113/jphysiol.1961.sp006803
- 1110 Dean, P. (1995). Modelling the role of the cerebellar fastigial nuclei in producing accurate saccades: the  
1111 importance of burst timing. *Neuroscience* 68, 1059–1077
- 1112 Dean, P., Mayhew, J. E., and Langdon, P. (1994). Learning and maintaining saccadic accuracy: a model of  
1113 brainstemcerebellar interactions. *Journal of Cognitive Neuroscience* 6, 117–138
- 1114 Dean, P. and Porrill, J. (2008). Adaptive filter models of the cerebellum: computational analysis. *Cerebellum*  
1115 7, 567–571
- 1116 Delgado, A., Sierra, A., Querejeta, E., Valdiosera, R., and Aceves, J. (1999). Inhibitory control of the  
1117 GABAergic transmission in the rat neostriatum by D2 dopamine receptors. *Neuroscience* 95, 1043–1048.  
1118 doi:10.1016/S0306-4522(99)00495-9
- 1119 DeLong, M., Crutcher, M. D., and Georgopoulos, A. (1985). Primate globus pallidus and subthalamic  
1120 nucleus: functional organization. *Journal of Neurphysiology* 53, 530–543
- 1121 Deubel, H. and Schneider, W. X. (1996). Saccade target selection and object recognition: Evidence for a  
1122 common attentional mechanism. *Vision Research* 36, 1827–1837. doi:10.1016/0042-6989(95)00294-4
- 1123 DeWolf, T., Stewart, T. C., Slotine, J.-J., and Eliasmith, C. (2016). A spiking neural model of adaptive arm  
1124 control. *Proceedings of the Royal Society B: Biological Sciences* 283, 20162134. doi:10.1098/rspb.2016.  
1125 2134
- 1126 Dorris, M. C., Paré, M., and Munoz, D. P. (1997). Neuronal Activity in Monkey Superior Colliculus  
1127 Related to the Initiation of Saccadic Eye Movements. *The Journal of Neuroscience* 17, 8566

- 1128 Edelman, J. A. and Keller, E. L. (1996). Activity of visuomotor burst neurons in the superior colliculus  
1129 accompanying express saccades. *Journal of Neurophysiology* 76, 908
- 1130 Federighi, P., Cevenini, G., Dotti, M. T., Rosini, F., Pretegiani, E., Federico, A., et al. (2011). Differences  
1131 in saccade dynamics between spinocerebellar ataxia 2 and late-onset cerebellar ataxias. *Brain* 134,  
1132 879–891. doi:10.1093/brain/awr009
- 1133 Fuchs, A. and Luschei, E. (1970). Firing patterns of abducens neurons of alert monkeys in relationship to  
1134 horizontal eye movement. *Journal of Neurophysiology* 33, 382–392
- 1135 Funahashi, S., Chafee, M. V., and Goldman-Rakic, P. S. (1993). Prefrontal neuronal activity in rhesus  
1136 monkeys performing a delayed anti-saccade task. *Nature* 365, 753
- 1137 Galvan, A. and Wichmann, T. (2008). Pathophysiology of Parkinsonism. *Clinical Neurophysiology* 119,  
1138 1459–1474. doi:10.1016/j.clinph.2008.03.017
- 1139 Gancarz, G. and Grossberg, S. (1998). A neural model of the saccade generator in the reticular formation.  
1140 *Neural Networks* 11, 1159–1174. doi:10.1016/S0893-6080(98)00096-3
- 1141 Gaymard, B., Ploner, C. J., Rivaud, S., Vermersch, A. I., and Pierrot-Deseilligny, C. (1998). Cortical  
1142 control of saccades. *Experimental Brain Research* 123, 159–163. doi:10.1007/s002210050557
- 1143 Gerfen, C. R., Engbar, T. M., Mahan, L. C., Susel, Z., Chase, T. N., Monsma, F. J., et al. (1990). D1 and  
1144 D2 dopamine receptor regulated gene-expression of striatonigral and striatopallidal neurons. *Science*  
1145 250, 1429–1432
- 1146 Ghitani, N., Bayguinov, P. O., Vokoun, C. R., McMahon, S., Jackson, M. B., and Basso, M. A. (2014).  
1147 Excitatory Synaptic Feedback from the Motor Layer to the Sensory Layers of the Superior Colliculus.  
1148 *The Journal of Neuroscience* 34, 6822–6833. doi:10.1523/JNEUROSCI.3137-13.2014
- 1149 Gian G. Mascetti and Jorge R. Arriagada (1981). Tectotectal interactions through the commissure of the  
1150 superior colliculi. An electrophysiological study. *Experimental Neurology* 71, 122–133
- 1151 Girard, B. and Berthoz, A. (2005). From brainstem to cortex: Computational models of saccade generation  
1152 circuitry. *Progress in Neurobiology* 77, 215–251. doi:10.1016/j.pneurobio.2005.11.001
- 1153 Goldberg, M. E. and Wurtz, R. H. (1972). Activity of superior colliculus in behaving monkey. I. Visual  
1154 receptive fields of single neurons. *J Neurophysiol* 35, 542–559
- 1155 Gonon, F. (1997). Prolonged and extrasynaptic excitatory action of dopamine mediated by D1 receptors in  
1156 the rat striatum in vivo. *The Journal of neuroscience : the official journal of the Society for Neuroscience*  
1157 17, 5972–8
- 1158 Goossens, H. (2006). Dynamic Ensemble Coding of Saccades in the Monkey Superior Colliculus. *Journal*  
1159 *of Neurophysiology* 95, 2326–2341. doi:10.1152/jn.00889.2005
- 1160 Goossens, H. and van Opstal, A. J. (2012). Optimal control of saccades by spatial-temporal activity patterns  
1161 in the monkey superior colliculus. *PLoS computational biology* 8, e1002508
- 1162 Groh, J. M. (2001). Converting neural signals from place codes to rate codes. *Biological cybernetics* 85,  
1163 159–165
- 1164 Groh, J. M. (2011). Effects of Initial Eye Position on Saccades Evoked by Microstimulation in the Primate  
1165 Superior Colliculus: Implications for Models of the SC Read-Out Process. *Frontiers in Integrative*  
1166 *Neuroscience* 4. doi:10.3389/fnint.2010.00130
- 1167 Gurney, K., Prescott, T. J., and Redgrave, P. (2001a). A computational model of action selection in the  
1168 basal ganglia. I. A new functional anatomy. *Biological cybernetics* 84, 401–10
- 1169 Gurney, K., Prescott, T. J., and Redgrave, P. (2001b). A computational model of action selection in the  
1170 basal ganglia. II. Analysis and simulation of behaviour. *Biological cybernetics* 84, 411–23
- 1171 Hallworth, N. E., Wilson, C. J., and Bevan, M. D. (2003). Apamin-sensitive small conductance calcium-  
1172 activated potassium channels, through their selective coupling to voltage-gated calcium channels, are

- critical determinants of the precision, pace, and pattern of action potential generation in rat subthalamic nucleus neurons in vitro. *The Journal of neuroscience* 23, 7525–7542
- Harsing, L. G. and Zigmond, M. J. (1997). Influence of dopamine on GABA release in striatum: evidence for D1-D2 interactions and non-synaptic influences. *Neuroscience* 77, 419–29
- Hazy, T. E., Frank, M. J., and O'Reilly, R. C. (2007). Towards an executive without a homunculus: computational models of the prefrontal cortex/basal ganglia system. *Philosophical Transactions of the Royal Society B: Biological Sciences* 362, 1601–1613. doi:10.1098/rstb.2007.2055
- Hepp, K. and Henn, V. (1983). Spatio-temporal recoding of rapid eye movement signals in the monkey paramedian pontine reticular formation (PPRF). *Experimental brain research* 52, 105–120
- Hepp, K., Van Opstal, A. J., Straumann, D., Hess, B. J., and Henn, V. (1993). Monkey superior colliculus represents rapid eye movements in a two-dimensional motor map. *Journal of neurophysiology* 69, 965–979
- Hernández-López, S., Bargas, J., Surmeier, D. J., Reyes, A., and Galarraga, E. (1997). D1 receptor activation enhances evoked discharge in neostriatal medium spiny neurons by modulating an L-type Ca<sub>2+</sub> conductance. *The Journal of neuroscience : the official journal of the Society for Neuroscience* 17, 3334–42
- Hikosaka, O., Takikawa, Y., and Kawagoe, R. (2000). Role of the basal ganglia in the control of purposive saccadic eye movements. *Physiological reviews* 80, 953–978
- Hikosaka, O. and Wurtz, R. H. (1983). Visual and oculomotor functions of monkey substantia nigra pars reticulata. IV. Relation of substantia nigra to superior colliculus. *Journal of neurophysiology* 49, 1285–301
- Howard, L. A. and Tipper, S. (1997). Hand deviations away from visual cues: indirect evidence for inhibition. *Experimental brain research* 113, 144–152
- Humphries, M. D. and Gurney, K. N. (2002). The role of intra-thalamic and thalamocortical circuits in action selection. *Network: Computation in Neural Systems* 13, 131–156
- INCF Task Force on Multi-Scale Modeling (2011). Network Interchange for Neuroscience Modeling Language (NineML)
- Isa, T. (2002). Intrinsic processing in the mammalian superior colliculus. *Current Opinion in Neurobiology* 12, 668–677. doi:10.1016/S0959-4388(02)00387-2
- Isa, T. and Hall, W. C. (2009). Exploring the Superior Colliculus In Vitro. *Journal of Neurophysiology* 102, 2581–2593. doi:10.1152/jn.00498.2009
- James, S., Bell, O. A., Nazli, M. A. M., Pearce, R. E., Spencer, J., Tyrrell, K., et al. (2017). Target-distractor synchrony affects performance in a novel motor task for studying action selection. *PLOS ONE* 12, e0176945. doi:10.1371/journal.pone.0176945
- Jayaraman, A., Batton, R. R., and Carpenter, M. B. (1977). Nigrotectal projections in the monkey: an autoradiographic study. *Brain research* 135, 147–152
- Jiang, H., Stein, B. E., and McHaffie, J. G. (2003). Opposing basal ganglia processes shape midbrain visuomotor activity bilaterally. *Nature* 423, 982–986. doi:10.1038/nature01698
- Kita, H. and Kitai, S. T. (1991). Intracellular study of rat globus pallidus neurons: membrane properties and responses to neostriatal, subthalamic and nigral stimulation. *Brain research* 564, 296–305
- Kleine, J. F. (2003). Saccade-Related Neurons in the Primate Fastigial Nucleus: What Do They Encode? *Journal of Neurophysiology* 90, 3137–3154. doi:10.1152/jn.00021.2003
- Kühn, A. A., Williams, D., Kupsch, A., Limousin, P., Hariz, M., Schneider, G.-H., et al. (2004). Event-related beta desynchronization in human subthalamic nucleus correlates with motor performance. *Brain : a journal of neurology* 127, 735–46. doi:10.1093/brain/awh106

- 1218 Latto, R. (1977). The effects of bilateral frontal eye-field, posterior parietal or superior collicular lesions  
1219 on brightness thresholds in the rhesus monkey. *Neuropsychologia* 15, 507–516
- 1220 Lee, C., Rohrer, W. H., and Sparks, D. L. (1988). Population coding of saccadic eye movements by neurons  
1221 in the superior colliculus. *Nature* 332, 357–360. doi:10.1038/332357a0
- 1222 Lefèvre, P., Quaia, C., and Optican, L. M. (1998). Distributed model of control of saccades by superior  
1223 colliculus and cerebellum. *Neural Networks* 11, 1175–1190
- 1224 Linden, R. and Perry, V. (1983). Massive retinotectal projection in rats. *Brain research* 272, 145–149
- 1225 Ling, L., Fuchs, A. F., Siebold, C., and Dean, P. (2007). Effects of initial eye position on saccade-related  
1226 behavior of abducens nucleus neurons in the primate. *Journal of Neurophysiology* 98, 3581–3599
- 1227 Lynch, J. C., Hoover, J. E., and Strick, P. L. (1994). Input to the primate frontal eye field from the substantia  
1228 nigra, superior colliculus, and dentate nucleus demonstrated by transneuronal transport. *Experimental*  
1229 *Brain Research* 100, 181–186
- 1230 Maes, P. (1989). *The dynamics of action selection* (Artificial Intelligence Laboratory, Vrije Universiteit  
1231 Brussel)
- 1232 Marcos, E. and Genovesio, A. (2016). Determining Monkey Free Choice Long before the Choice Is Made:  
1233 The Principal Role of Prefrontal Neurons Involved in Both Decision and Motor Processes. *Frontiers in*  
1234 *Neural Circuits* 10. doi:10.3389/fncir.2016.00075
- 1235 Marino, R. A., Trappenberg, T. P., Dorris, M., and Munoz, D. P. (2012). Spatial Interactions in the Superior  
1236 Colliculus Predict Saccade Behavior in a Neural Field Model. *Journal of Cognitive Neuroscience* 24,  
1237 315–336. doi:10.1162/jocn\_a\_00139
- 1238 Mays, L. E. and Sparks, D. L. (1980). Dissociation of visual and saccade-related responses in superior  
1239 colliculus neurons. *Journal of Neurophysiology* 43, 207–232
- 1240 McCarthy, M. M., Moore-Kochlacs, C., Gu, X., Boyden, E. S., Han, X., and Kopell, N. (2011). Striatal  
1241 origin of the pathologic beta oscillations in Parkinson's disease. *Proceedings of the National Academy*  
1242 *of Sciences* 108, 11620–11625. doi:10.1073/pnas.1107748108
- 1243 McFarland, N. R. and Haber, S. N. (2002). Thalamic relay nuclei of the basal ganglia form both reciprocal  
1244 and nonreciprocal cortical connections, linking multiple frontal cortical areas. *Journal of Neuroscience*  
1245 22, 8117–8132
- 1246 McIlwain, J. T. (1982). Lateral spread of neural excitation during microstimulation in intermediate gray  
1247 layer of cat's superior colliculus. *Journal of Neurophysiology* 47, 167–178
- 1248 McPeek, R. M. (2006). Incomplete Suppression of Distractor-Related Activity in the Frontal Eye Field  
1249 Results in Curved Saccades. *Journal of Neurophysiology* 96, 2699–2711. doi:10.1152/jn.00564.2006
- 1250 McPeek, R. M., Han, J. H., and Keller, E. L. (2003). Competition Between Saccade Goals in the Superior  
1251 Colliculus Produces Saccade Curvature. *Journal of Neurophysiology* 89, 2577–2590. doi:10.1152/jn.  
1252 00657.2002
- 1253 McPeek, R. M. and Keller, E. L. (2002). Saccade Target Selection in the Superior Colliculus During a  
1254 Visual Search Task. *Journal of Neurophysiology* 88, 2019–2034
- 1255 Meredith, M. A. and Ramoa, A. S. (1998). Intrinsic Circuitry of the Superior Colliculus: Pharmacophysiological  
1256 Identification of Horizontally Oriented Inhibitory Interneurons. *Journal of Neurophysiology* 79,  
1257 1597–1602
- 1258 Middleton, F. A. and Strick, P. L. (2000). Basal ganglia and cerebellar loops: motor and cognitive circuits.  
1259 *Brain Research Reviews* 31, 236–250. doi:10.1016/S0165-0173(99)00040-5
- 1260 Mink, J. (1996). The basal ganglia: Focused selection and inhibition of competing motor programs.  
1261 *Progress in Neurobiology* 50, 381–425

- 1262 Mink, J. W. and Thach, W. T. (1993). Basal ganglia intrinsic circuits and their role in behavior. *Current  
1263 opinion in Neurobiology* 3, 950–957
- 1264 Mitchinson, B., Chan, T.-S., Chambers, J., Pearson, M., Humphries, M., Fox, C., et al. (2010). BRAHMS:  
1265 Novel middleware for integrated systems computation. *Advanced Engineering Informatics* 24, 49–61.  
1266 doi:10.1016/j.aei.2009.08.002
- 1267 Mitchinson, B. and James, S. S. (2015). BRAHMS. RRID: SCR\_015642
- 1268 Monosov, I. E., Trageser, J. C., and Thompson, K. G. (2008). Measurements of simultaneously recorded  
1269 spiking activity and local field potentials suggest that spatial selection emerges in the frontal eye field.  
1270 *Neuron* 57, 614–625
- 1271 Morén, J., Shibata, T., and Doya, K. (2013). The Mechanism of Saccade Motor Pattern Generation  
1272 Investigated by a Large-Scale Spiking Neuron Model of the Superior Colliculus. *PLoS ONE* 8, e57134.  
1273 doi:10.1371/journal.pone.0057134
- 1274 Munoz, D. P. (2002). Commentary: Saccadic eye movements: overview of neural circuitry. In *Progress in  
1275 Brain Research*, ed. D. M. J. Hyona, W. Heide and R. Radach (Elsevier), vol. Volume 140. 89–96
- 1276 Munoz, D. P. and Everling, S. (2004). Look away: the anti-saccade task and the voluntary control of eye  
1277 movement. *Nature Reviews Neuroscience* 5, 218–228. doi:10.1038/nrn1345
- 1278 Nambu, A., Yoshida, S.-i., and Jinnai, K. (1990). Discharge patterns of pallidal neurons with input from  
1279 various cortical areas during movement in the monkey. *Brain Research* 519, 183–191. doi:10.1016/  
1280 0006-8993(90)90076-N
- 1281 N'Guyen, S., Thurat, C., and Girard, B. (2014). Saccade learning with concurrent cortical and subcortical  
1282 basal ganglia loops. *Frontiers in Computational Neuroscience* 8. doi:10.3389/fncom.2014.00048
- 1283 Norman, D. A. and Shallice, T. (1986). Attention to action. In *Consciousness and self-regulation* (Springer).  
1284 1–18
- 1285 Nowotny, T. (2011). Flexible neuronal network simulation framework using code generation for NVidia®  
1286 CUDA™. *BMC Neuroscience* 12, P239. doi:10.1186/1471-2202-12-S1-P239
- 1287 Nowotny, T., Cope, A. J., Yavuz, E., Stimberg, M., Goodman, D. F., Marshall, J., et al. (2014). SpineML  
1288 and Brian 2.0 interfaces for using GPU enhanced Neuronal Networks (GeNN). *BMC Neuroscience* 15,  
1289 P148. doi:10.1186/1471-2202-15-S1-P148
- 1290 Olivier, E., Corvisier, J., Pauluis, Q., and Hardy, O. (2000). Evidence for glutamatergic tectotectal neurons  
1291 in the cat superior colliculus: a comparison with GABAergic tectotectal neurons. *European Journal of  
1292 Neuroscience* 12, 2354–2366
- 1293 Ottes, F. P., Van Gisbergen, J. A., and Eggermont, J. J. (1986). Visuomotor fields of the superior colliculus:  
1294 A quantitative model. *Vision Research* 26, 857–873. doi:10.1016/0042-6989(86)90144-6
- 1295 Papapavlou, C. and Moustakas, K. (2014). Physics-based modelling and animation of saccadic eye  
1296 movement
- 1297 Parent, A. and Hazrati, L. (1993). Anatomical aspects of information processing in primate basal ganglia.  
1298 *Trends in Neuroscience* 16, 111–116
- 1299 Quaia, C., Lefèvre, P., and Optican, L. M. (1999). Model of the Control of Saccades by Superior Colliculus  
1300 and Cerebellum. *Journal of Neurophysiology* 82, 999
- 1301 Quaia, C., Paré, M., Wurtz, R. H., and Optican, L. M. (2000). Extent of compensation for varia-  
1302 tions in monkey saccadic eye movements. *Experimental Brain Research* 132, 39–51. doi:10.1007/  
1303 s002219900324
- 1304 Redgrave, P., Prescott, T. J., and Gurney, K. (1999). The basal ganglia: a vertebrate solution to the selection  
1305 problem? *Neuroscience* 89, 1009–1023

- 1306 Reppert, T. R., Lempert, K. M., Glimcher, P. W., and Shadmehr, R. (2015). Modulation of Saccade  
1307 Vigor during Value-Based Decision Making. *Journal of Neuroscience* 35, 15369–15378. doi:10.1523/  
1308 JNEUROSCI.2621-15.2015
- 1309 Richmond, P. (2015). DAMSON
- 1310 Richmond, P., Cope, A., Gurney, K., and Allerton, D. J. (2014). From Model Specification to Simulation  
1311 of Biologically Constrained Networks of Spiking Neurons. *Neuroinformatics* 12, 307–323. doi:10.1007/  
1312 s12021-013-9208-z
- 1313 Robinson, D. (1972). Eye movements evoked by collicular stimulation in the alert monkey. *Vision Research*  
1314 12, 1795–1808. doi:10.1016/0042-6989(72)90070-3
- 1315 Robinson, D. A. (1975). Oculomotor control signals. In *Basic mechanisms of ocular motility and their*  
1316 *clinical implications*, eds. G. Lennerstrand and P. Bach-y Rita (Oxford: Pergamon). 337–374
- 1317 Robinson, D. A. and Fuchs, A. F. (1969). Eye movements evoked by stimulation of frontal eye fields.  
1318 *Journal of Neurophysiology* 32, 637–648
- 1319 Rovamo, J. and Virsu, V. (1979). An estimation and application of the human cortical magnification factor.  
1320 *Experimental Brain Research* 37, 495–510. doi:10.1007/BF00236819
- 1321 Sabes, P. N., Breznen, B., and Andersen, R. A. (2002). Parietal representation of object-based saccades.  
1322 *Journal of Neurophysiology* 88, 1815–1829
- 1323 Saint-Cyr, J. A., Ungerleider, L. G., and Desimone, R. (1990). Organization of visual cortical inputs to the  
1324 striatum and subsequent outputs to the pallidonigral complex in the monkey. *Journal of Comparative*  
1325 *Neurology* 298, 129–156
- 1326 Schall, J. D., Hanes, D. P., Thompson, K. G., and King, D. J. (1995). Saccade target selection in frontal  
1327 eye field of macaque .1. Visual and premovement activation. *Journal of Neuroscience* 15, 6905–6918
- 1328 Schall, J. D. and Thompson, K. G. (1999). Neural selection and control of visually guided eye movements.  
1329 *Annual review of neuroscience* 22, 241–259
- 1330 Schiller, P. H., Sandell, J. H., and Maunsell, J. H. (1987). The effect of frontal eye field and superior  
1331 colliculus lesions on saccadic latencies in the rhesus monkey. *Journal of Neurophysiology* 57, 1033
- 1332 Schlag, J. D. (2002). Neurons that program what to do and in what order. *Neuron* 34, 177–178
- 1333 Schwartz, E. L. (1977). Spatial mapping in the primate sensory projection: Analytic structure and relevance  
1334 to perception. *Biological Cybernetics* 25, 181–194. doi:10.1007/BF01885636
- 1335 Schwartz, E. L. (1980). Computational anatomy and functional architecture of striate cortex: A spatial  
1336 mapping approach to perceptual coding. *Vision Res.* 20, 645–669
- 1337 Schweighofer, N., Arbib, M. A., and Dominey, P. F. (1996). A model of the cerebellum in adaptive control  
1338 of saccadic gain. *Biological Cybernetics* 75, 19–28
- 1339 Scudder, C. A. (1988). A new local feedback model of the saccadic burst generator. *J Neurophysiol* 59,  
1340 1454
- 1341 Segraves, M. A. and Goldberg, M. E. (1987). Functional properties of corticotectal neurons in the  
1342 monkey{' }s frontal eye field. *Journal of Neurophysiology* 58, 1387–1419
- 1343 Seth, A., Sherman, M., Reinbolt, J. a., and Delp, S. L. (2011). OpenSim: a musculoskeletal modeling  
1344 and simulation framework for in silico investigations and exchange. *Procedia IUTAM* 2, 212–232.  
1345 doi:10.1016/j.piutam.2011.04.021
- 1346 Slotnick, S. D., Klein, S. A., Carney, T., and Sutter, E. E. (2001). Electrophysiological estimate of human  
1347 cortical magnification. *Clinical Neurophysiology* 112, 1349–1356
- 1348 Sommer, M. A. and Wurtz, R. H. (2000). Composition and topographic organization of signals sent from  
1349 the frontal eye field to the superior colliculus. *Journal of Neurophysiology* 83, 1979–2001

- 1350 Sparks, D. L. (2002). The brainstem control of saccadic eye movements. *Nature Reviews Neuroscience* 3,  
1351 952–964. doi:10.1038/nrn986
- 1352 Sparks, D. L. and Nelson, I. S. (1987). Sensory and motor maps in the mammalian superior colliculus.  
1353 *Trends in Neurosciences* 10, 312–317. doi:10.1016/0166-2236(87)90085-3
- 1354 Stanton, G. B., Goldberg, M. E., and Bruce, C. J. (1988a). Frontal eye field efferents in the macaque  
1355 monkey: I. Subcortical pathways and topography of striatal and thalamic terminal fields. *Journal of  
1356 Comparative Neurology* 271, 473–492. doi:10.1002/cne.902710402
- 1357 Stanton, G. B., Goldberg, M. E., and Bruce, C. J. (1988b). Frontal eye field efferents in the macaque  
1358 monkey: II. Topography of terminal fields in midbrain and pons. *The Journal of Comparative Neurology*  
1359 271, 493–506. doi:10.1002/cne.902710403
- 1360 Sterling, P. (1971). Receptive fields and synaptic organization of the superficial gray layer of the cat  
1361 superior colliculus. *Vision Research* 11, 309–IN47. doi:10.1016/0042-6989(71)90048-4
- 1362 Tabareau, N., Bennequin, D., Berthoz, A., Slotine, J.-J., and Girard, B. (2007). Geometry of the superior  
1363 colliculus mapping and efficient oculomotor computation. *Biological cybernetics* 97, 279–292
- 1364 Takagi, M., Zee, D. S., and Tamargo, R. J. (1998). Effects of Lesions of the Oculomotor Vermis on Eye  
1365 Movements in Primate: Saccades. *Journal of Neurophysiology* 80, 1911
- 1366 Talbot, S. and Marshall, W. (1941). Physiological Studies on Neural Mechanisms of Visual Localization  
1367 and Discrimination\*. *American Journal of Ophthalmology* 24, 1255–1264. doi:10.1016/S0002-9394(41)  
1368 91363-6
- 1369 Tehovnik, E. J., Sommer, M. A., Chou, I.-H., Slocum, W. M., and Schiller, P. H. (2000). Eye fields in the  
1370 frontal lobes of primates. *Brain Research Reviews* 32, 413–448. doi:10.1016/S0165-0173(99)00092-2
- 1371 Thelen, D. G. (2003). Adjustment of Muscle Mechanics Model Parameters to Simulate Dynamic  
1372 Contractions in Older Adults. *Journal of Biomechanical Engineering* 125, 70. doi:10.1115/1.1531112
- 1373 Thivierge, J.-P. and Marcus, G. F. (2007). The topographic brain: from neural connectivity to cognition.  
1374 *Trends in Neurosciences* 30, 251–259. doi:10.1016/j.tins.2007.04.004
- 1375 Thompson, K. G. and Bichot, N. P. (2005). A visual salience map in the primate frontal eye field. In  
1376 *Progress in Brain Research*, ed. A. v. O. G. J. A. R. a. P. R. R. M. K. J. van Pelt, C. N. Levelt (Elsevier),  
1377 vol. 147 of *Development, Dynamics and Pathology of Neuronal Networks: from Molecules to Functional  
1378 Circuits*. 249–262
- 1379 Thompson, K. G., Bichot, N. P., and Sato, T. R. (2005). Frontal eye field activity before visual search errors  
1380 reveals the integration of bottom-up and top-down salience. *Journal of Neurophysiology* 93, 337–351
- 1381 Thurat, C., NGuyen, S., and Girard, B. (2015). Biomimetic race model of the loop between the superior  
1382 colliculus and the basal ganglia: Subcortical selection of saccade targets. *Neural Networks* 67, 54–73.  
1383 doi:10.1016/j.neunet.2015.02.004
- 1384 Tipper, S. P., Howard, L. A., and Paul, M. A. (2001). Reaching affects saccade trajectories. *Experimental  
1385 Brain Research* 136, 241–249
- 1386 Van Gisbergen, J., Van Opstal, A., and Tax, A. (1987). Collicular ensemble coding of saccades based on  
1387 vector summation. *Neuroscience* 21, 541–555. doi:10.1016/0306-4522(87)90140-0
- 1388 Van Gisbergen, J. A. M., Van Opstal, A. J., and Schoenmakers, J. J. M. (1985). Experimental test of two  
1389 models for the generation of oblique saccades. *Experimental brain research* 57, 321–336
- 1390 van Opstal, A. J. and Goossens, H. H. L. M. (2008). Linear ensemble-coding in midbrain superior colliculus  
1391 specifies the saccade kinematics. *Biological Cybernetics* 98, 561–577. doi:10.1007/s00422-008-0219-z
- 1392 Van Opstal, A. J., Hepp, K., Hess, B. J., Straumann, D., and Henn, V. (1991). Two-rather than three-  
1393 dimensional representation of saccades in monkey superior colliculus. *Science* 252, 1313–1315

- 1394 van Opstal, A. J. and van Gisbergen, J. A. (1990). Role of monkey superior colliculus in saccade averaging.  
1395 *Experimental Brain Research* 79, 143–149
- 1396 Vokoun, C. R., Huang, X., Jackson, M. B., and Basso, M. A. (2014). Response Normalization in the  
1397 Superficial Layers of the Superior Colliculus as a Possible Mechanism for Saccadic Averaging. *Journal*  
1398 *of Neuroscience* 34, 7976–7987. doi:10.1523/JNEUROSCI.3022-13.2014
- 1399 Vokoun, C. R., Jackson, M. B., and Basso, M. A. (2010). Intralaminar and Interlaminar Activity within the  
1400 Rodent Superior Colliculus Visualized with Voltage Imaging. *Journal of Neuroscience* 30, 10667–10682.  
1401 doi:10.1523/JNEUROSCI.1387-10.2010
- 1402 Vokoun, C. R., Jackson, M. B., and Basso, M. A. (2011). Circuit dynamics of the superior colliculus  
1403 revealed by in vitro voltage imaging: Vokoun et al. *Annals of the New York Academy of Sciences* 1233,  
1404 41–47. doi:10.1111/j.1749-6632.2011.06166.x
- 1405 Waitzman, D. M., Ma, T. P., Optican, L. M., and Wurtz, R. H. (1991). Superior colliculus neurons mediate  
1406 the dynamic characteristics of saccades. *Journal of Neurophysiology* 66, 1716–1737
- 1407 Walker, R., Deubel, H., Schneider, W. X., and Findlay, J. M. (1997). Effect of remote distractors on saccade  
1408 programming: evidence for an extended fixation zone. *Journal of neurophysiology* 78, 1108–1119
- 1409 Wickens, J. (1997). Basal ganglia: structure and computations. *Network: Computation in Neural Systems*  
1410 8, 77–109
- 1411 Wilson, C. and Kawaguchi, Y. (1996). The origins of the two-state spontaneous membrane potential  
1412 fluctuations of neostriatal spiny neurons. *The Journal of Neuroscience* 16, 2397–2410
- 1413 Wilson, C. J. (2004). A Model of Reverse Spike Frequency Adaptation and Repetitive Firing of Subthalamic  
1414 Nucleus Neurons. *Journal of Neurophysiology* 91, 1963–1980. doi:10.1152/jn.00924.2003
- 1415 Wu, H. H., Williams, C. V., and McLoon, S. C. (1994). Involvement of nitric oxide in the elimination  
1416 of a transient retinotectal projection in development. *SCIENCE-NEW YORK THEN WASHINGTON-*,  
1417 1593–1593
- 1418 Wurtz, R. H. and Albano, J. E. (1980). Visual-motor function of the primate superior colliculus. *Annual*  
1419 *review of Neuroscience* 3, 189–226. doi:10.1146/annurev.ne.03.030180.001201
- 1420 Wurtz, R. H. and Goldberg, M. E. (1972). Activity of superior colliculus in behaving monkey. III. Cells  
1421 discharging before eye movements. *J Neurophysiol* 35, 575–586

## FIGURES

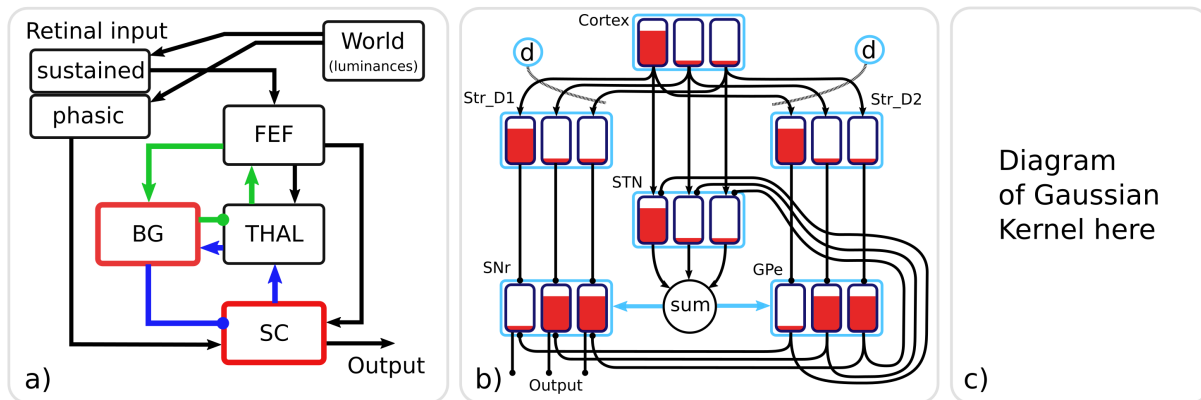


**Figure 6. a) The macroscopic architecture of the Cope-Chambers model.** The main nuclei modelled as brain systems are: basal ganglia (BG), frontal eye fields (FEF), thalamus (THAL) and superior colliculus (SC). The retinal input is presented via non-biologically plausible retinal populations. The loops through basal ganglia, which define the architecture, are shown with coloured lines: the cortical loop (through FEF and THAL) in green and the sub-cortical loop (through SC and THAL) in blue. Connections with arrowheads indicate excitatory connections, those with circles are inhibitory. A red border indicates that the box represents a sub-system of two or more populations; a black box indicates (at least, within the context of the model) a single neural population. The BG box is expanded in: **b) The basal ganglia model component.** This shows a basal ganglia comprising striatum (Str\_D1 & Str\_D2), subthalamic nucleus (STN), globus pallidum externum (GPe) and substantia nigra reticulata (SNr). The model has three action channels shown as black boxes within each blue population border. Three channels of cortical input to the BG are also depicted. Red indicates the activation level of a given channel, helping to illustrate the selection mechanism. For example, the channel indicated by the leftmost bar has a high salience (cortical input) and excites activity in Str\_D1 which then inhibits the leftmost bar in SNr. The diffuse projection from STN is equivalent to summing its projections channel-wise, and then projecting the sum to all channels of its target populations (the blue arrows indicate that all channels of GPe and SNr are targeted by the connection). Dopaminergic modulation of the inputs to the striatum are indicated by the blue circles labelled 'd' and the dotted lines. The SNr sends inhibitory output projections to its targets.

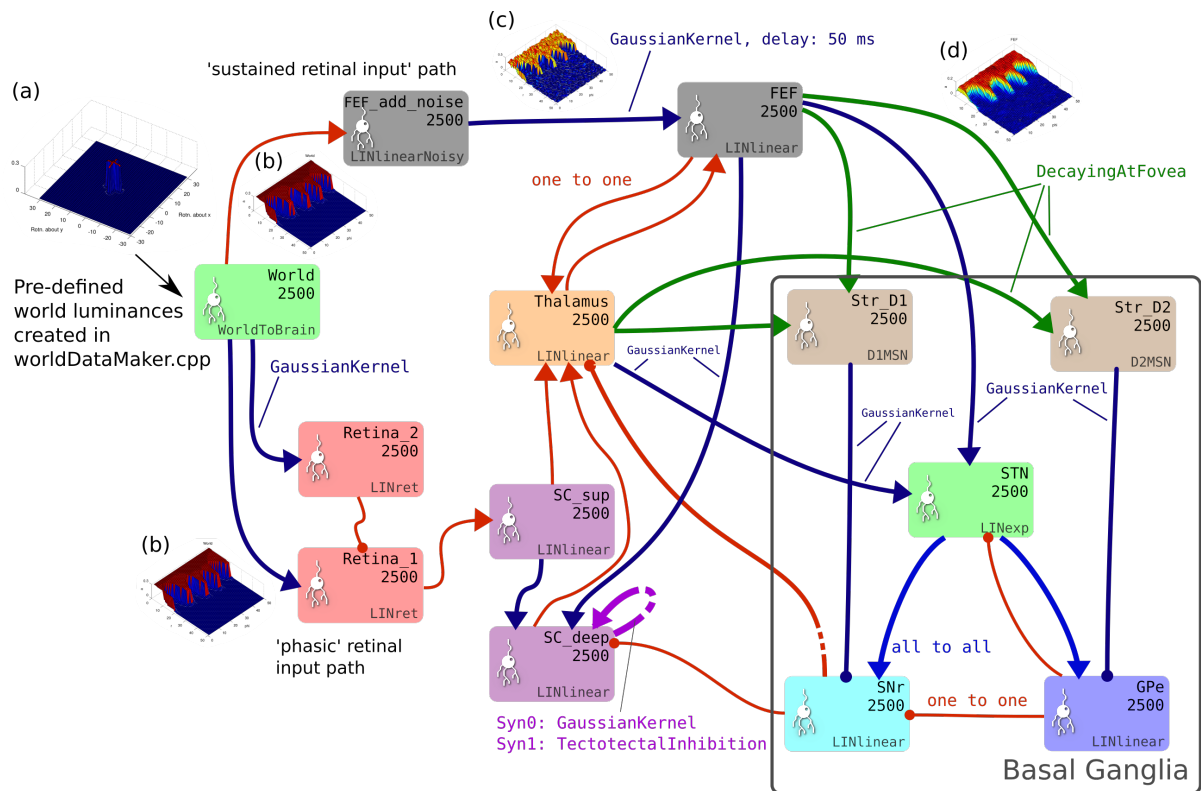


**Figure 7.** The brain model. This is the SpineCreator ‘network layer’ view of the model. Each box represents a neural population with 2500 elements, arranged in a  $50 \times 50$  grid. The SpineML component name is printed on the bottom right corner of each population box and the population name is at the top. The overall connectivity between populations is represented by the projection arrows with the colour indicating the connectivity scheme (one-to-one connections are red, Gaussian kernel connections are dark blue and so on). Excitatory connections have arrowheads and inhibitory connections have circles, although for details of the behaviour of the connections, the weight-update and post-synapse components must be studied. Briefly, the model comprises a *World* population, into which a retinotopically organised view of the world is introduced. This information is passed into cortical populations (FEF) and subcortical populations (SC) via a simple model of the retina. These feed a cortico-thalamo-basal ganglia loop, which selects which region of the deep layer of superior colliculus should be disinhibited, allowing activity to build up therein. The five populations comprising the basal ganglia are enclosed in a grey outline. Note that substantia nigra pars compacta is not modelled here, instead the level of dopamine in the striatum is set via a parameter in the Str\_D1 and Str\_D2 populations

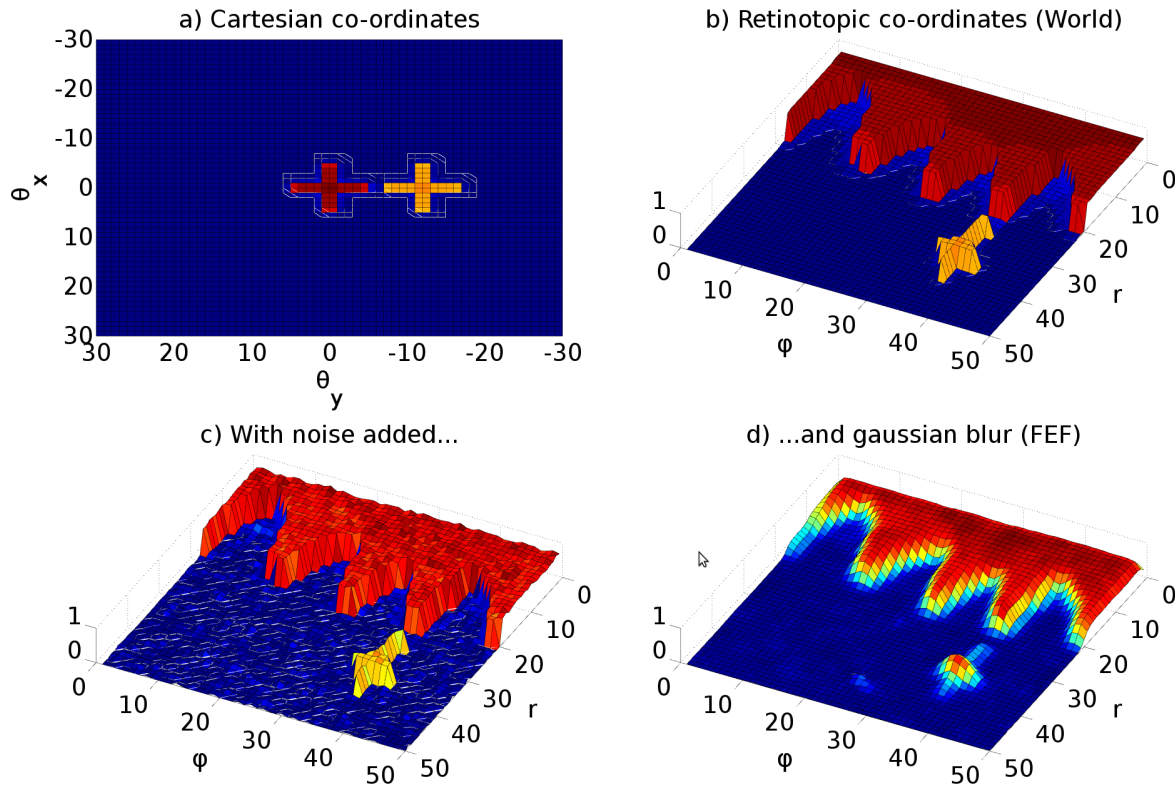


**Figure 8.** Representative mapping from eye's frame of reference in Cartesian co-ordinates to retinotopic co-ordinates. (a) The mapping of luminances in the eye's frame of reference. The world input is pre-defined by a JSON configuration file. Luminance position, size and shape can be defined in this file, along with the times at which luminances appear and disappear. The worldDataMaker.cpp code computes the locations of the luminances in the eye's frame of reference, given its rotational state. It also computes a 2D Gaussian convolution of the luminances. Here, there are two cross shaped luminances spanning  $10^\circ$ , one of value 0.8 at the fixation point (0,0) and one of value 0.5 at a peripheral position (0,- $12^\circ$ ). Note that these crosses have the same 'bar width' of  $2^\circ$  as the crosses used in the simulations, but their span of  $10^\circ$  is greater than the  $6^\circ$  used in the simulations, to make these images clearer. (b) The locations of the luminances in the eye's frame of reference are then converted into retinotopic co-ordinates, with centrally located luminances being represented at low values of  $r$  and more peripheral luminances having higher values of  $r$ .  $\phi$  encodes rotational angle: 1 and 50 encode upward movement; 13 is left; 25 is down; 37 is right. The output of the World component is fed into FEF\_add\_noise and into the retinal neuron populations. The colour map makes it possible to distinguish between the two crosses. (c) The FEF\_add\_noise populations adds a level of noise to the signal representing processing of the signal in visual cortex. (d) A Gaussian projection from FEF\_add\_noise to FEF further blurs the activity in FEF. FEF is the input to the basal ganglia and one input to superior colliculus.

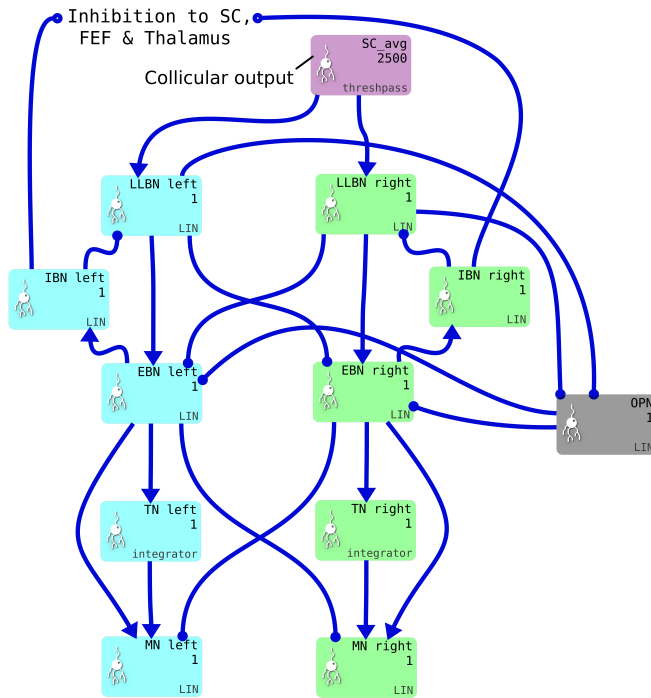


**Figure 9.** One pair of channels of the saccadic burst generator (SBG) for left (cyan) or right (green) movements. Collicular activity in SC\_avg excites the channels via SBG weight maps. Each box represents a neural population and shows the population name, the number of neural elements (here 2500 or 1) and the SpineML component name; *LIN* for Leaky integrator or *integrator*. Key: LLBN: Long lead burst neurons; IBN: Inhibitory burst neurons; OPN: Omnipause neurons; EBN: Excitatory burst neurons; TN: Tonic neurons; MN: Motoneurons.

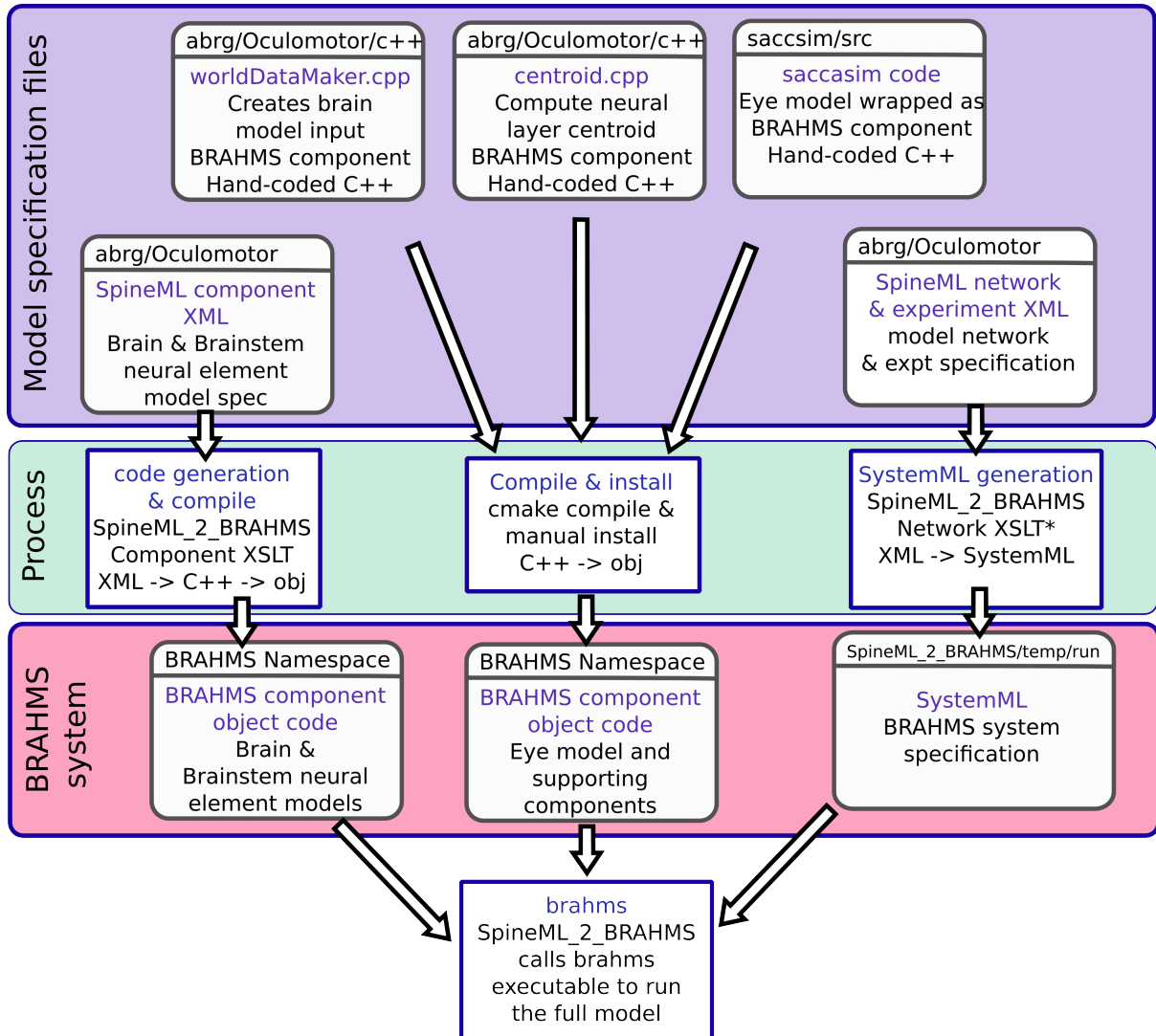


**Figure 10.** The model framework. The model is specified using a combination of declarative XML files and hand-coded C++. These original model specifications are shown within the blue box. b) The green box shows the processes which are applied to the model specification to produce the BRAHMS system. Most of the process is defined within the scripts which make up SpineML\_2\_BRAHMS, but the hand-written components must be manually compiled and installed within the BRAHMS Namespace, allowing the BRAHMS executable to locate them at runtime. c) The red box shows the resulting BRAHMS system ready to be executed by the BRAHMS executable. In practice, this call is made by SpineML\_2\_BRAHMS.

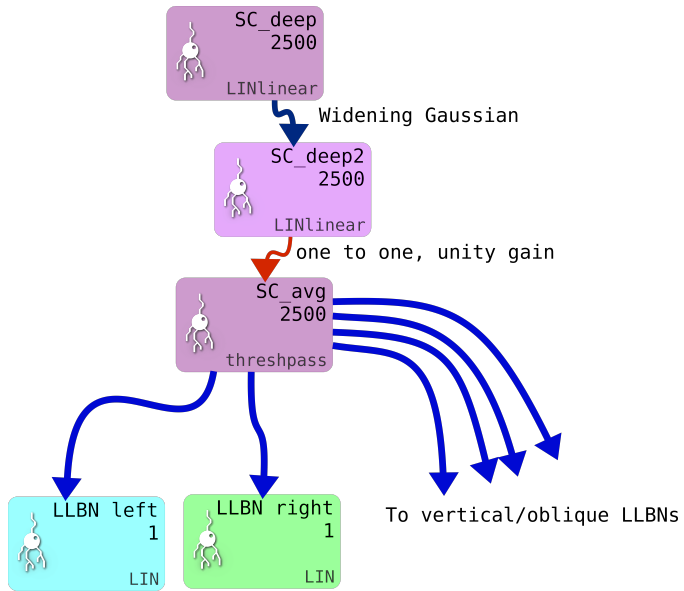


**Figure 11.** Showing the additional deep layer of superior colliculus (SC\_deep2) and the output layer (SC\_avg, named for the fact that in an earlier version of the model, it received the output of the centroid of SC\_deep). The widening Gaussian projection is shown as the arrow between SC\_deep and SC\_deep2.

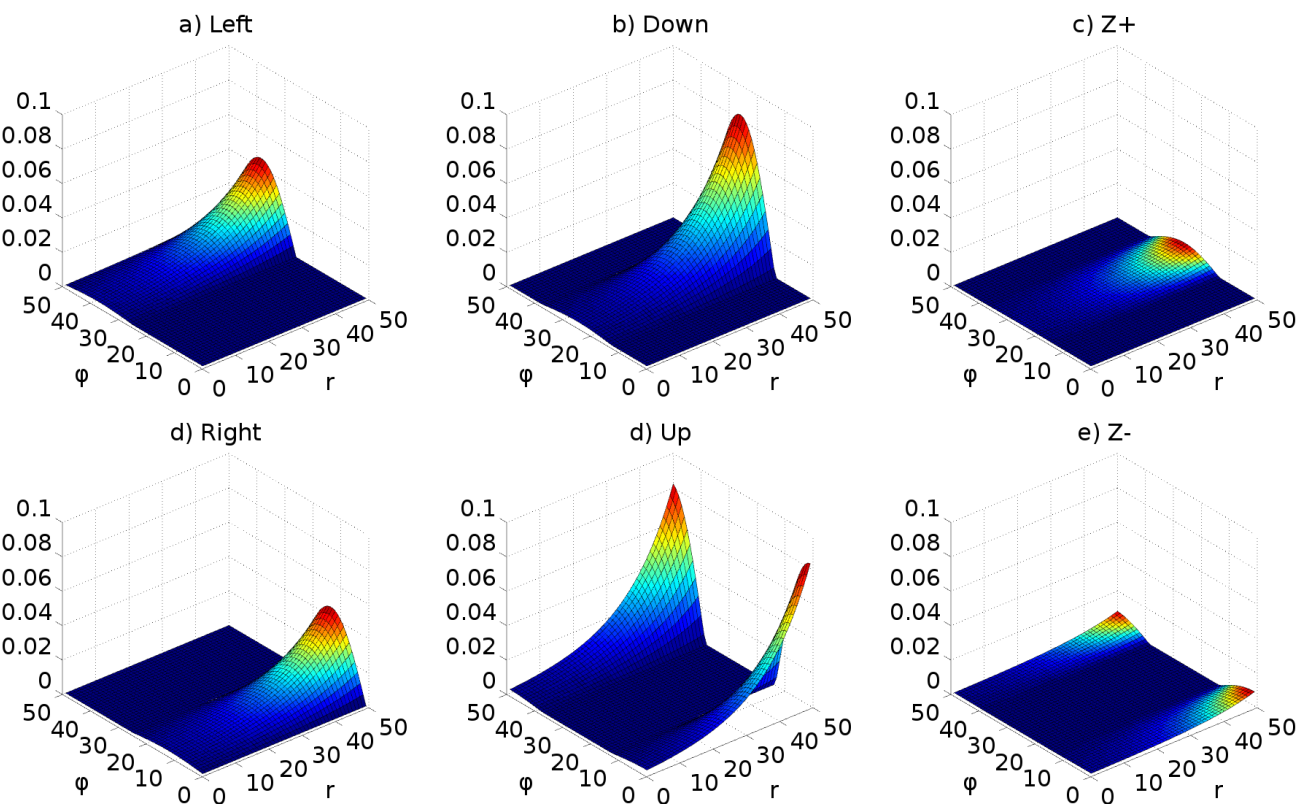


**Figure 13.** Weight maps for the connections between the output layer of superior colliculus and the six long lead burst neurons of the saccadic burst generator model. Each map increases exponentially with increasing  $r$ , multiplied by  $\cosine(\phi)$  about its ‘active’ axis.

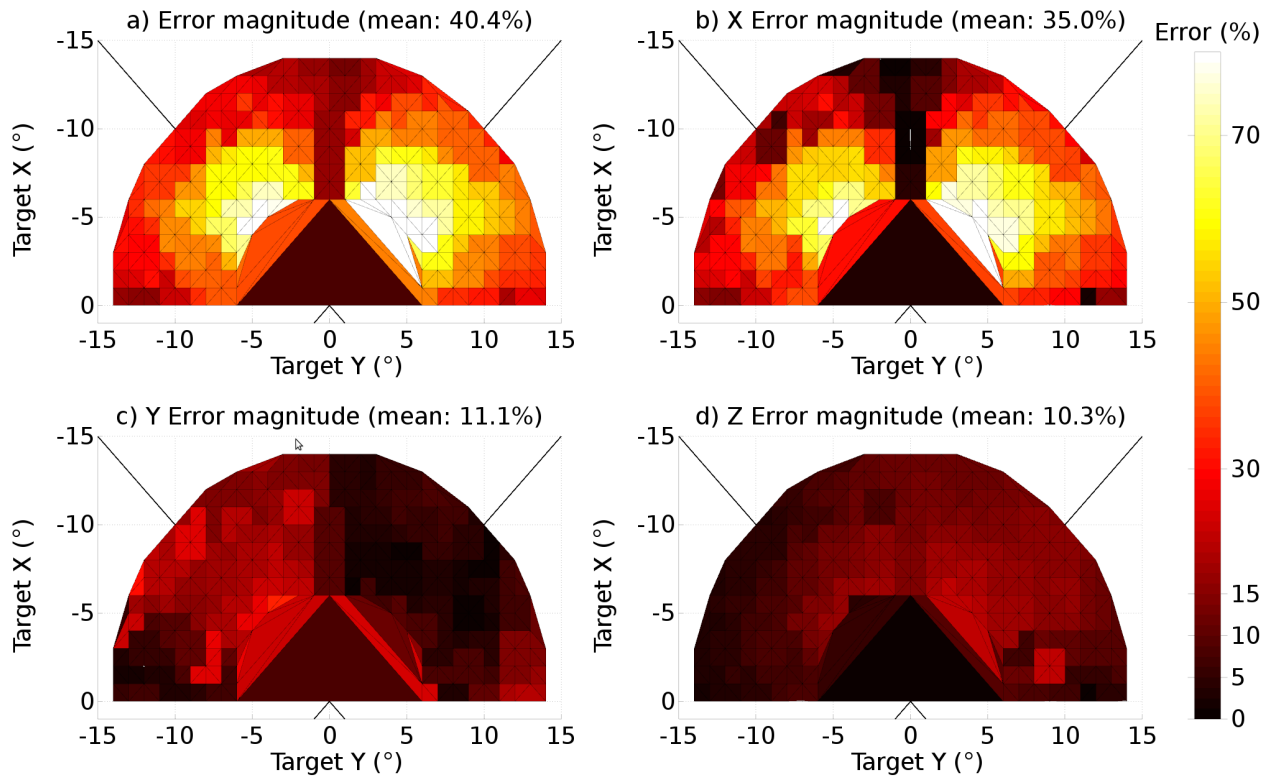


**Figure 14.** The end-point error surface for the original, naïve model (TModel3). a) The ratio of the magnitudes of the total error vector and the target vector, expressed as a percentage. b) The ratio of the magnitude of the  $x$  component of the error vector to the magnitude of the target vector, expressed as a percentage. c) As (b) but for the  $y$  component. d) As (b), for  $z$  component. All colour maps are shown with the same scale. The target rotations,  $\theta_x^t$  and  $\theta_y^t$  are denoted ‘Target X’ and ‘Target Y’ in the figure.

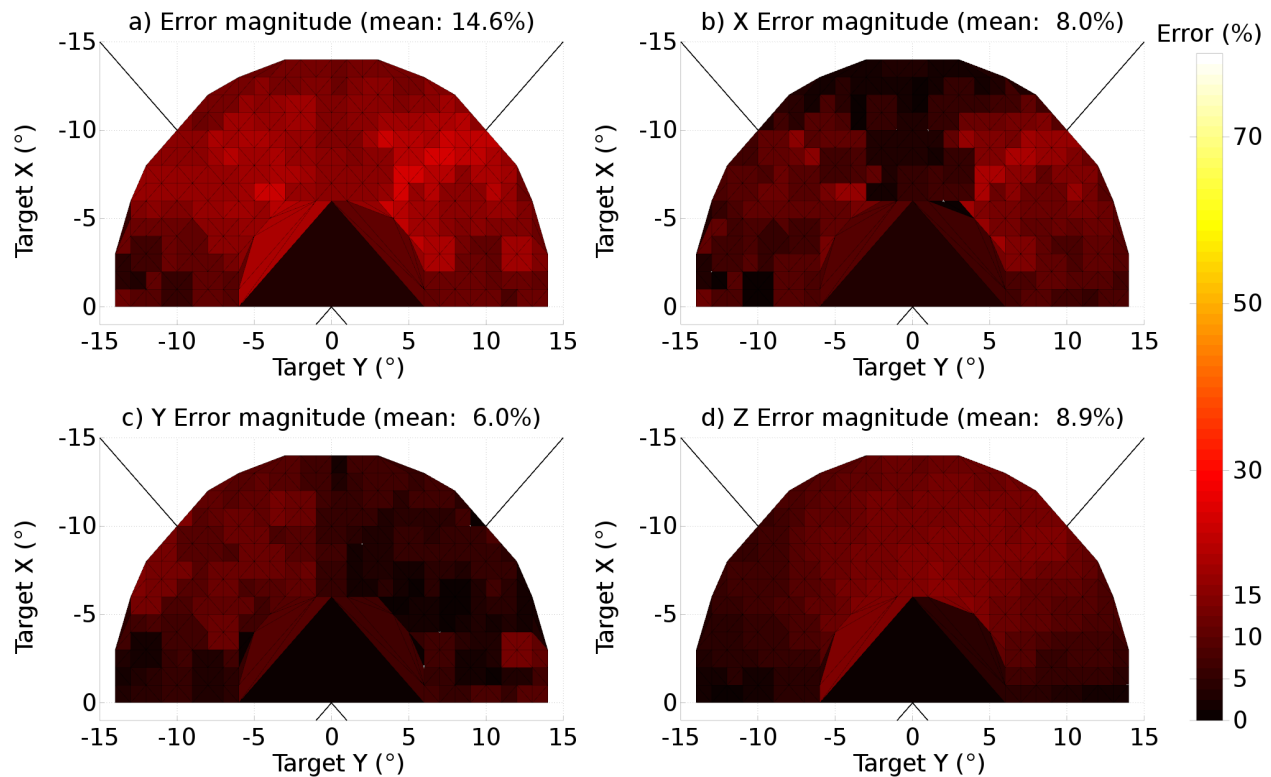


**Figure 15.** The end-point error surface for the model in which a widening projection field was added to the model of the superior colliculus. a) The ratio of the magnitudes of the total error vector and the target vector, expressed as a percentage. b) The ratio of the magnitude of the  $x$  component of the error vector to the magnitude of the target vector, expressed as a percentage. c) As (b) but for the  $y$  component. d) As (b), for  $z$  component. All colour maps are shown with the same scale. The target rotations,  $\theta_x^t$  and  $\theta_y^t$  are denoted ‘Target X’ and ‘Target Y’ in the figure. Note that the range of the colour scale is 0 to 20%, a much smaller range than the range in Fig 14.

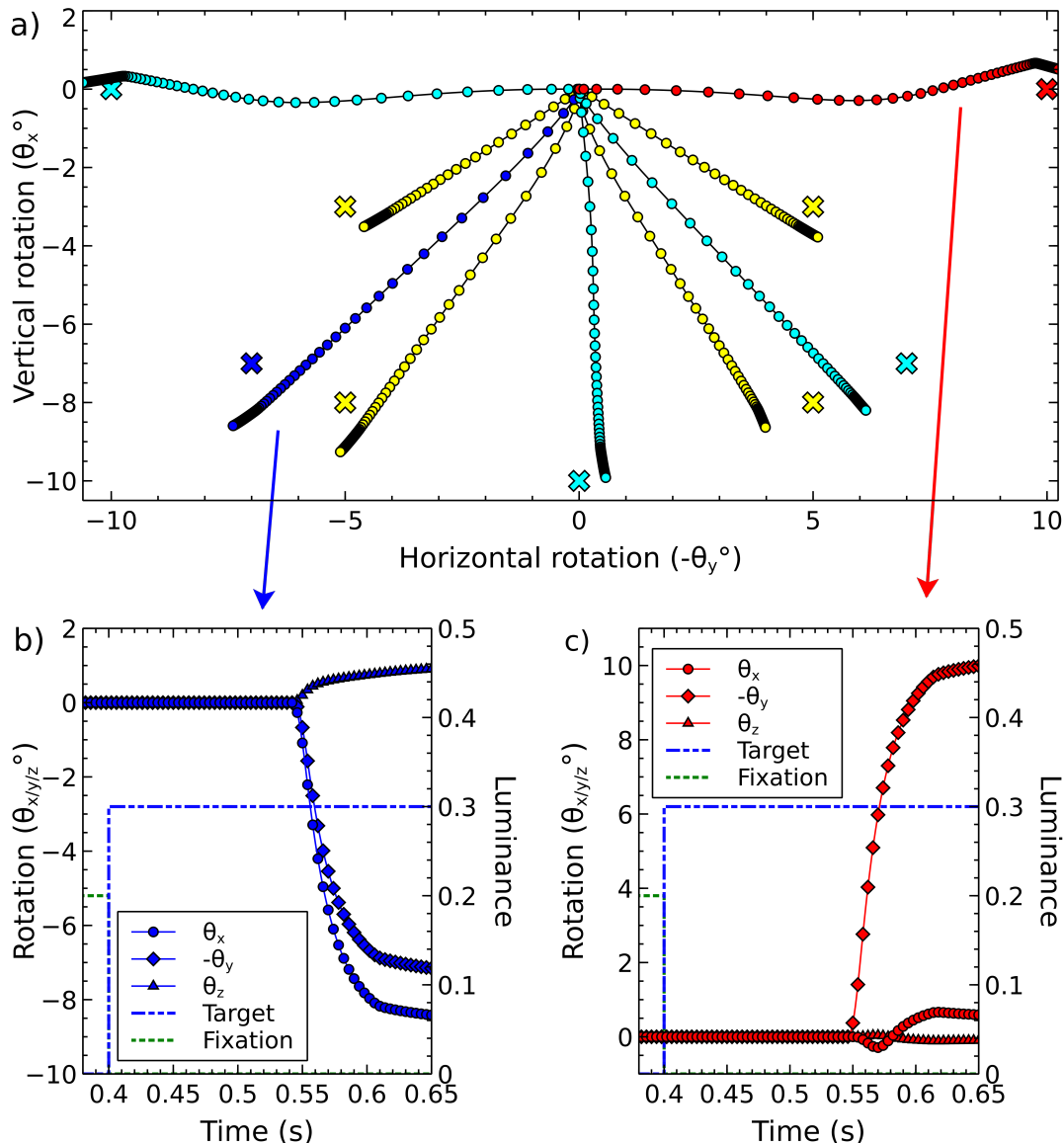


**Figure 16.** Representative single saccades. a) Trajectories from 9 saccades to a single target at 9 different locations. In each case, a fixation cross luminance of magnitude 0.2 was displayed at (0,0), the start position of the eye, until time 0.4 s. The target luminance, magnitude 0.3 was illuminated at time 0.4 s. Trajectory shape is dependent on the target position, and there is a variable amount of error in the end-points achieved by the model. Colour is used in this diagram as an aid to distinguishing different saccades and their targets; for a given saccade, the target location is given by the cross of the same colour closest to the end of the trajectory. b) The three rotational components of the ‘blue’ saccade, to target location (-7,-7). c) The three rotational components of the ‘red’ saccade, to target location (0,-10).

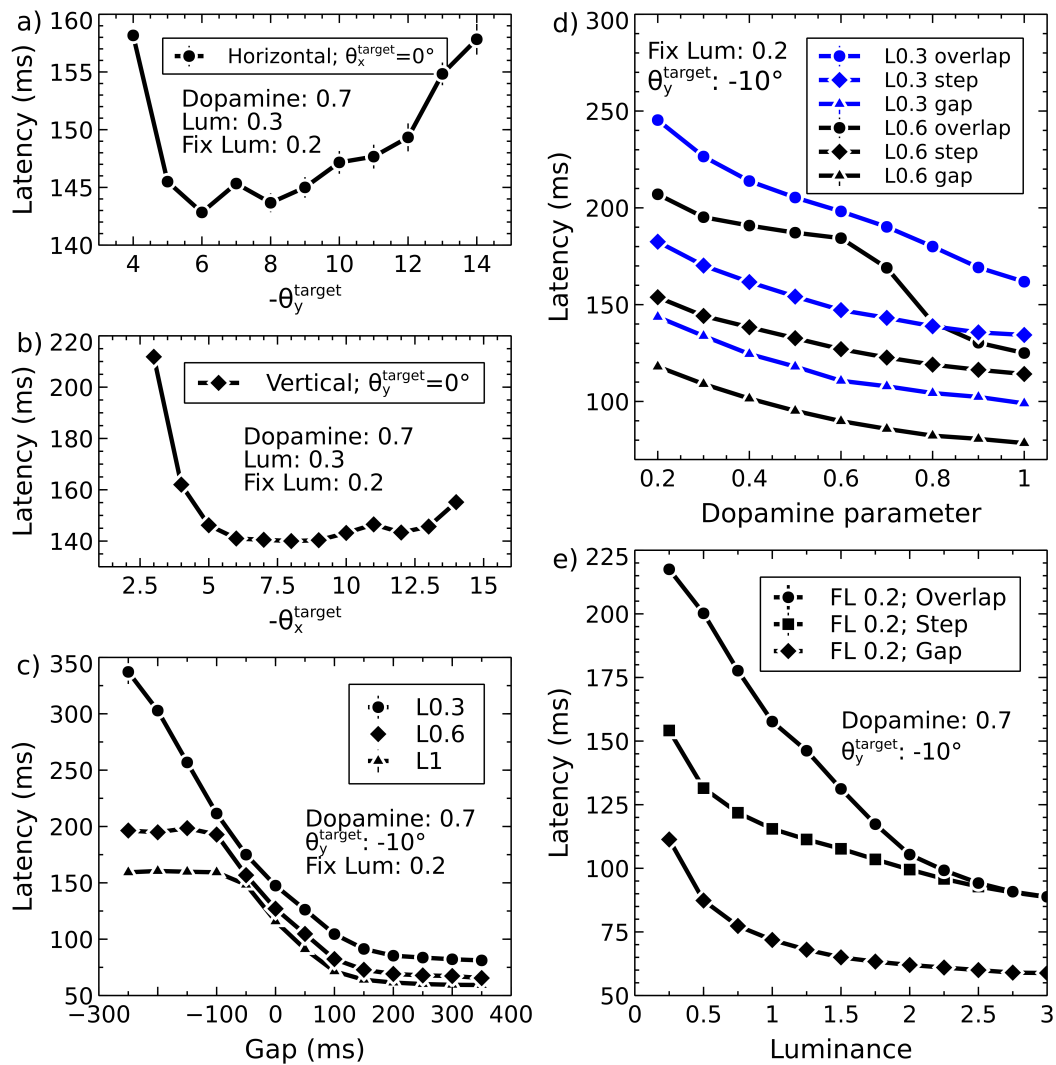


**Figure 17.** Exploring saccade latencies. a) Latency to first movement as a function of target eccentricity for horizontal targets. b) Latency vs. eccentricity for vertical targets. c) Latency vs. gap at three different luminance values. d) The effect of the dopamine parameter on saccade latencies in gap, step and overlap conditions, for two different target luminances. e) Saccade vs. luminance showing gradual transition between reflexive and express behaviour.

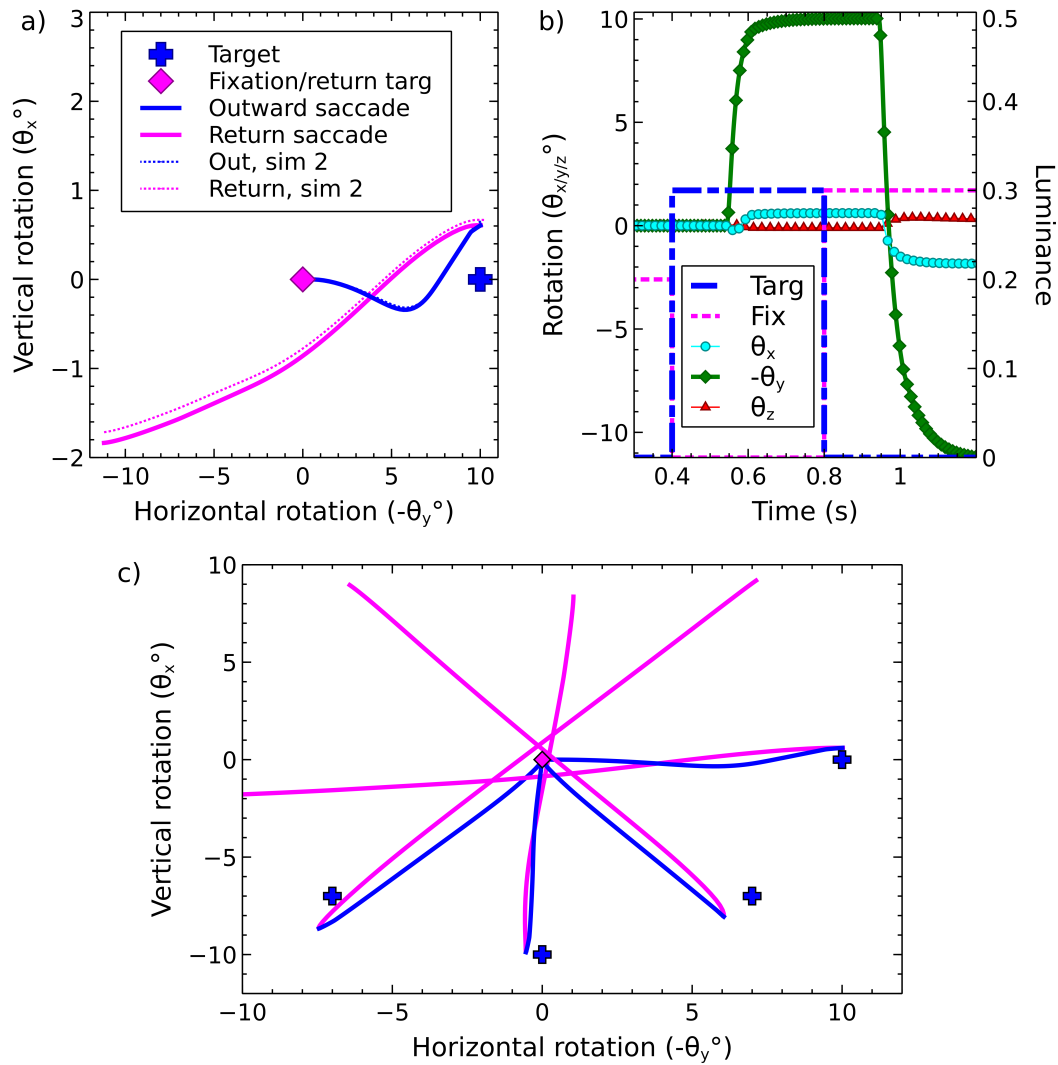


**Figure 18.** There and back - a saccade to a target, followed by return to the original fixation. a) Out and return saccade to a target at (0, -10°) b) Rotational components of the saccade shown in (a). c) Outward and return trajectories for the saccade shown in (a) alongside saccades to three other targets.

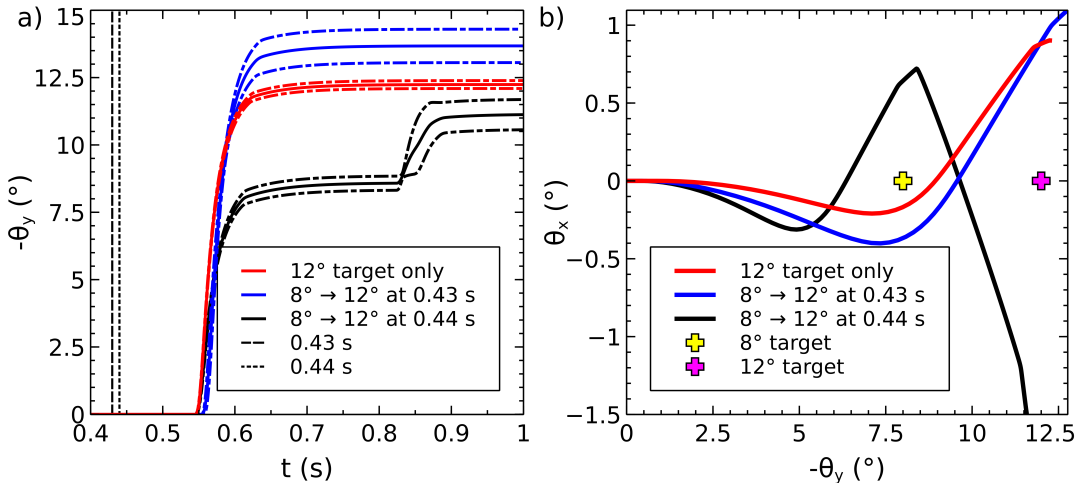


**Figure 19.** Double steps. The effect of illuminating a first target at  $8^\circ$  or  $12^\circ$ , followed by a second target at  $12^\circ$  or  $8^\circ$ . a) Horizontal rotation of the eye plotted vs. time for a saccade to the  $12^\circ$  target only (red), and to an  $8^\circ$  target at 0.4 s followed by a  $12^\circ$  target after 30 ms (blue) or 40 ms (black). The timings are indicated by vertical lines. When the second target is presented up to 30 ms after the initial target, the initial target has not had time to dominate the output saccade and a saccade to a location close to the second target is made. If the delay is 40 ms or more, the activity from the initial target has time to cause a built up of activity in SC\_deep and an initial saccade close to the first target is made, followed, after a longer than usual latency period, with a second saccade closer to the second target. In this graph, the mean of five separate simulations is plotted along with  $\pm 1$  standard deviation around the mean. b) The  $\theta_x/\theta_y$  trajectories corresponding to the data presented in (a).